Arctic Report Card 2017

Arctic shows no sign of returning to reliably frozen region of recent past decades

2017 Headlines

Arctic shows no sign of returning to reliably frozen region of recent past decades

Despite relatively cool summer temperatures, observations in 2017 continue to indicate that the Arctic environmental system has reached a 'new normal', characterized by long-term losses in the extent and thickness of the sea ice cover, the extent and duration of the winter snow cover and the mass of ice in the Greenland Ice Sheet and Arctic glaciers, and warming sea surface and permafrost temperatures.

Video

Highlights

- The average **surface air temperature** for the year ending September 2017 is the 2nd warmest since 1900; however, cooler spring and summer temperatures contributed to a rebound in snow cover in the Eurasian Arctic, slower summer sea ice loss, and below-average melt extent for the Greenland ice sheet.
- The **sea ice cover** continues to be relatively young and thin with older, thicker ice comprising only 21% of the ice cover in 2017 compared to 45% in 1985.
- In August 2017, **sea surface temperatures** in the Barents and Chukchi seas were up to 4° C warmer than average, contributing to a delay in the autumn freeze-up in these regions.
- Pronounced increases in **ocean primary productivity**, at the base of the marine food web, were observed in the Barents and Eurasian Arctic seas from 2003 to 2017.
- Arctic **tundra** is experiencing increased greenness and record permafrost warming.
- Pervasive changes in the environment are influencing **resource management** protocols, including those established for fisheries and wildfires.
- The unprecedented rate and global reach of Arctic change disproportionally affect the **people of northern communities**, further pressing the need to prepare for and adapt to the new Arctic.

December 2017

www.arctic.noaa.gov/Report-Card

Table of Contents

Executive Summary

J. Richter-Menge[1], J. E. Overland[2], J. T. Mathis[3], E. Osborne[3]

[1]University of Alaska Fairbanks, Institute of Northern Engineering, Fairbanks, AK, USA

[2]National Oceanic and Atmospheric Administration, Pacific Marine Environmental Laboratory, Seattle, WA, USA

[3]National Oceanic and Atmospheric Administration, Arctic Research Program, Silver Spring, MD, USA

The Arctic Report Card (www.arctic.noaa.gov/Report-Card/), going into its 12th year, considers a range of environmental observations throughout the Arctic, and is updated annually. As in previous years, the 2017 update highlights the changes that continue to occur in, and among, the physical and biological components of the Arctic environmental system.

Arctic conditions in 2017 provide an excellent example of the need to assess observations in the context of longer-term records. After a very warm Arctic-wide autumn 2016, spring and summer 2017 had near average air temperatures relative to the 1981-2010 climatology. These spring/summer conditions were reminiscent of conditions before the long-term temperatures increases that began in the 1990s. These 'relatively cool' temperatures in spring and summer 2017 contributed to a rebound in the snow cover extent in Eurasia during May and June, a slowing of the summer sea ice loss, and below-average melt extent for the Greenland ice sheet.

Taken alone, observations made in spring and summer 2017 might encourage a relaxation in the concerns over environmental conditions in the Arctic. However, when taken in context, there are many strong signals that continue to indicate that the Arctic environmental system has reached a 'new normal'. While modulated by natural variability in regional and seasonal fluctuations, this 'new normal' is characterized by Arctic air temperatures that are warming at double the rate of the global temperature increase. Accordingly, there are pronounced decade-long declines in the extent and volume of the sea ice cover, the extent and duration of the winter snow cover, and the mass of the Greenland Ice Sheet and Arctic glaciers. Temperatures are increasing in the surface of the Arctic Ocean, contributing to later formation of the sea ice cover in the autumn. Temperatures are also increasing in the permafrost on the adjacent continents. Arctic paleo-reconstructions, which extend back millions of years, indicate that the magnitude and pace of the 21st century sea-ice decline and surface ocean warming is unprecedented in at least the last 1,500 years and likely much longer.

The persistence of the environmental conditions that define the Arctic's 'new normal' has enabled increases in Arctic Ocean primary productivity, which forms the basis of the marine food web. Additionally, above ground vegetation is also expanding and affecting hydrological dynamics, carbon and nutrient cycling, the surface energy balance, and the habits of wild and domesticated plant eaters. The pervasive changes in the environment influence resource management protocols, including those established for fisheries and wildfires, and directly affecting the people living in Arctic communities. The unprecedented rate and global reach of these changes highlight the pressing need to prepare for and adapt to the New Arctic, enabled by more effective and timely communication of observations to scientists, policymakers, and residents.

Detailed Highlights from Arctic Report Card 2017

- The second warmest (after 2016) surface air temperature anomaly (+1.6° C relative to 1981-2010) north of 60° N since the year 1900 was observed between October 2016 and September 2017.
- On the 7th of March 2017 satellites observed the lowest winter maximum in sea ice on record (1979-present). The March maximum was 8% lower and the September minimum was 25% lower than the 1981-2010 average sea ice extent. The sea ice cover continues to be relatively young and thin with multiyear ice (more than 1 year old) comprising only 21% of ice cover in 2017 compared to 45% in 1985.
- Sea surface temperature in the Chukchi Sea, northwest of Alaska, has experienced the largest warming trend: ~0.7° C per decade since 1982. In August 2017 the Barents and Chukchi seas experienced surface temperatures up to 4° C warmer than the 1982-2010 average.
- The most pronounced increasing trends in ocean primary productivity during the 2003-2017 period were observed in the Barents Sea and Eurasian Arctic regions. Long-term records reveal that years with elevated ocean productivity levels are often associated with earlier sea ice breakup during the spring/summer transition.
- The downward trend in total ice mass of the Greenland ice sheet averaged over the last 15 years is estimated at 264-270 Gt/yr. The spatial extent of melt for the period June, July and August 2017 reached a maximum of 32.9%, marking the lowest maximum extent since 1996.
- Spring snow cover extent over Eurasia in May 2017 was the 2nd highest recorded by satellite observations dating back to 1967. May and June snow cover extent anomalies over the Eurasian Arctic mark the first positive anomalies observed since 2005 and 2004, respectively.
- Tundra greenness has increased substantially throughout the Arctic during 2015 and 2016 (the most recent year with a complete data set) following 3-4 years of continuous declines. Peak tundra greenness for 2016 ranks 4th (entire Arctic), 9th (Eurasian Arctic), and 3rd (North American Arctic) in the context of the 35-year satellite record.
- Permafrost temperatures in 2016 (the most recent set of complete observations) at many observation sites around the Arctic were among the highest on record (as long as 1978-present, but duration of records vary). Increases in permafrost temperature, since 2000, have been greatest in cold permafrost of the Alaskan Arctic, Canadian high Arctic, and Svalbard.

Acknowledgments

November 17, 2017

Surface Air Temperature

J. E. Overland[1], E. Hanna[2], I. Hanssen-Bauer[3], S. -J. Kim[4], J. E. Walsh[5], M. Wang[6], U. S. Bhatt[7], R. L. Thoman[8]

[1]NOAA/Pacific Marine Environmental Laboratory, Seattle, WA, USA

[2]Department of Geography, University of Lincoln, Lincoln, UK

[3]Norwegian Meteorological Institute, Blindern, 0313 Oslo, Norway

[4]Korea Polar Research Institute, Incheon, Republic of Korea

[5]International Arctic Research Center, University of Alaska Fairbanks, Fairbanks, AK, USA

[6]Joint Institute for the Study of the Atmosphere and Ocean, University of Washington, Seattle, WA, USA

[7]Geophysical Institute, University of Alaska Fairbanks, Fairbanks, AK, USA

[8]NOAA, National Weather Service, Alaska Region, Anchorage, AK, USA

Highlights

- The average annual surface air temperature anomaly over land north of 60° N for October 2016-September 2017 was the second highest (after 2015-2016), in the observational record beginning in 1900.
- Arctic air temperature continues to increase at double the rate of the global mean air temperature increase.
- Extreme Arctic-wide air high temperatures were observed in autumn 2016 (October-December); extensive regions over the central Arctic showed anomalies exceeding +5° C. These conditions were primarily due to southerly winds moving warm air into the Arctic from the mid-latitude Pacific and Atlantic oceans.
- Neutral temperature anomalies occurred across the central Arctic Ocean with weak sea level pressure gradients. Like summer 2016, summer 2017 weather conditions did not support rapid summer sea ice and ice sheet loss.

Arctic surface air temperature is an indicator of regional and global climate change. Although there are year-to-year and regional differences in air temperatures due to natural variability, the magnitude and Arctic-wide character of the long-term temperature increase is a major indicator of global warming and the influence of increases in greenhouse gases (Overland, 2009; Notz and Stroeve, 2016). We report on the spatial and temporal variability of Arctic air temperatures during the period October 2016 through September 2017, the 12-month period since the end of the previous reporting period in Arctic Report Card 2016.

After a very warm autumn across the Arctic 2016 and a warm winter on the Asian side, spring and summer 2017 had near-average air temperatures relative to the 1981-2010 climatology. Spring and summer 2017 temperatures were reminiscent of conditions (see essay on *Terrestrial Snow Cover*) before the long-term temperatures increases that began in the 1990s. The impact of the 2017 spring and summer conditions is seen throughout the contributions in Arctic Report Card 2017. For instance, there was more snow in spring and less sea ice and ice sheet melt in summer. The 2017 fire season was not unusual. Unlike many recent years of the previous decade, where high sea level pressure dominated the Arctic region, weak low pressure systems were observed in spring

and summer 2017. The latter is more consistent with atmospheric and wind forcing patterns typically observed prior to 2007 (Overland et al., 2017), and runs counter to the conditions driving the longer-term trends reported throughout Arctic Report Card 2017.

Mean Annual Land Surface Air Temperature

At +1.6° C, the mean annual surface air temperature (SAT) anomaly for October 2016-September 2017 for land stations north of 60° N is the second highest value (after 2016) in the record starting in 1900 (**Fig. 1**). Currently, the Arctic is warming at more than twice the rate of global mean temperatures (**Fig. 1**).
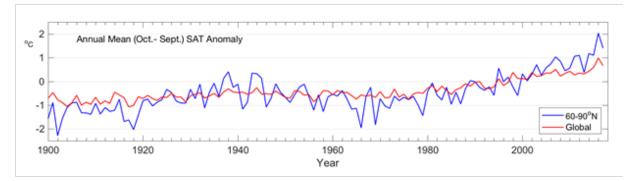

Fig. 1. Arctic (land stations north of 60° N) and global mean annual land surface air temperature (SAT) anomalies (in °C) for the period 1900-2017 relative to the 1981-2010 mean value. Note that there were few stations in the Arctic, particularly in northern Canada, before 1940. The data are from the CRUTEM4 dataset, which is available at www.cru.uea.ac.uk/cru/data/temperature/.

The greater rate of Arctic temperature increase, compared to the global mean increase, is referred to as Arctic Amplification. Mechanisms for Arctic Amplification include: reduced summer albedo, due to sea ice and snow cover loss; the increase of total water vapor content in the Arctic atmosphere; a summer decrease and winter increase in total cloudiness (Makshtas et al., 2011; Lenaerts et al., 2017); the additional heat generated by newly sea-ice free ocean areas that are maintained later into the autumn (Serreze and Barry, 2011); and the lower rate of heat loss to space in the Arctic relative to the subtropics, due to lower mean surface temperatures in the Arctic (Pithan and Mauritsen, 2014). Arctic warming has also been influenced by past air pollution reductions in Europe (Acosta Navarro et al., 2016).

Seasonal Surface Air Temperature Variation

Seasonal air temperature variations are divided into autumn 2016 (October, November, December [OND]), and winter (January, February, March [JFM]), spring (April, May, June [AMJ]), and summer (July, August, September [JAS]) of 2017. These seasonal SAT divisions are chosen to coincide with the seasonal cycles of key Arctic variables: summer sea ice minimum occurs in September and autumn cooling continues through December.

Fig. 2. Seasonal anomaly patterns for near-surface air temperatures (in °C) relative to the baseline period 1981-2010 in autumn 2016 (top left), winter 2017 (top right), spring 2017 (bottom left), and summer 2017 (bottom right). Temperature anomalies are from slightly above the surface layer (at 925 mb level) to emphasize large spatial patterns rather than local features. Data for this and the following figures are from NOAA/ESRL, Boulder, CO, at https://www.esrl.noaa.gov/psd/.

Autumn 2016 (OND). A broad swath of extreme warm temperature anomalies (> +5° C) stretched across the central Arctic (**Fig. 2a**). The warmest temperature extremes, north of Bering Strait and near the North Pole, were due to advection of warm air from the south from the Pacific and Atlantic oceans (see Arctic and Mid-latitudes Connections, below). Svalbard Airport reported an all-time high monthly average for October (+3.2°C; 1.8° above the previous record from year 2000). Iceland was also notably mild, while Greenland coastal temperatures were unexceptional. Warm temperature anomalies in Alaska led to a late start to winter snow pack (see essay on *Terrestrial Snow Cover*).

Winter 2017 (JFM). Most of the remaining year from January through September was uneventful in terms of major features on a seasonal basis (**Fig. 2b-d**). There were, however, notable short term, regional temperature anomalies in response to highly variable jet stream shapes. For instance, Iceland experienced a record high maximum temperature for February (Trausti Jonsson, Icelandic Met Office, pers. comm.). March 2017 had major warmth across Siberia (**Fig 3**) including east Asia. Even though Arctic-mid-latitude weather connections are hypothesized for eastern Asia due to loss of sea ice the Kara-Barents Sea (Kim et al., 2014) there were no severe cold storms in Asia during the 2017 winter.

Spring 2017 (AMJ). Spring (**Fig. 2c**) showed some warm temperature anomalies in the East Siberian Sea, a continuation of the warm feature observed in March. This regional warming supported early sea ice loss in the Chukchi Sea (see essay on *Sea Ice*). May saw anomalous high pressure extend between Greenland and Norway, with relatively warm but unexceptional temperatures over Greenland, and the warmest May for 25 years over the UK.

Summer 2017 (JAS). Like Summer 2016, Summer 2017 contrasted with warm conditions in much of the previous decade (**Fig. 2d**). Neutral anomalies occurred across the central Arctic in summer 2017, which did not support continued overall rapid summer sea ice loss (see essay on *Sea Ice*). Mean coastal Greenland temperatures were near climatological levels, in contrast to some summers in the recent decade. Alaska/northwestern Canada was the only region with above average summer SAT. Several locations in the interior of Alaska had the warmest calendar month of record in July, yet Alaska had a normal wildfire season overall (see essay on *Wildfires*). Many stations in the north and east of Iceland recorded record temperatures for September.

Fig. 3. March 2017 air temperatures with extremes over Siberia. Source: https://www.esrl.noaa.gov/psd/.

Arctic and Mid-latitudes Connections

Like winter 2016, warm temperature conditions in the Arctic in autumn 2016 were primarily a response to southerly winds advecting warm air into the Arctic from mid-latitudes. The positive near-surface air temperature anomalies were associated with a persistent pattern in the geopotential height field characterized by low values west of Greenland and over eastern Siberia and higher values in the central Arctic (**Fig. 4a**). Winds tend to follow the contours of geopotential heights counter-clockwise around low values. Consequently, warm air over the northeast Pacific Ocean was advected into and across Alaska and the seas north of Alaska and eastern Russia. Warm

southerly winds from the North Atlantic also extended across the central Arctic past the North Pole (i.e., follow purple contours in **Fig. 4a**), providing the primary atmospheric source of anomalous warmth over much of the Arctic Ocean.

Normally there is a single large Arctic region of low geopotential heights, which establish a tropospheric polar vortex (see, for example, Overland et al., 2015). In Autumn 2016 higher geopotential heights in the central Arctic split the polar vortex into two pieces. The persistence of warm Arctic temperatures into the late autumn was in part caused by a positive feedback, where advection of warm air temperatures and delay of autumn freeze-up of sea ice contributed to increasing the temperatures and the geopotential heights over the central Arctic, which in turn helped to maintain the unusual 2016 wind pattern.

After December 2016 the tropospheric polar vortex, as shown by the geopotential height field, varied considerably by month and region. For example, the height field for March (**Fig 4b**), which supported a warm Siberia by advecting warm air from the Atlantic Ocean region (**Fig 3**), has an entirely different shape than it did in autumn (**Fig 4a**).

Summer sea level pressure (**Fig 5**) was characterized by low pressures in the central Arctic. This pattern prevented extra heat from mid-latitudes from penetrating into the central Arctic and differed from low sea-ice summers. This pressure pattern was accompanied by widespread cloud cover as seen in satellite observations that limited the solar heating of the lower atmosphere in the central Arctic. These conditions are likely to have contributed to a slowing of the sea ice loss in summer 2017 (see essay on *Sea Ice*).

Fig. 4a. Geopotential height (700 mb) from October-December 2016. The normally continuous tropospheric polar vortex of low heights (purple shading) over the central Arctic was split in two parts in autumn 2016, similar to winter 2016 (see 2016 Arctic Report Card). The jet stream is located where the gradient in the geopotential height is large. This pattern gives rise to southerly winds and extreme record temperatures over the central Arctic.

Fig. 4b. Geopotential height field for March 2017 showing a different tropospheric jet stream structure (dark blue contours) than autumn 2016 (**Fig. 4a**).

Fig. 5. Sea level pressure field for summer 2017.

References

Acosta Navarro, J. C., et al., 2016: Amplification of Arctic warming by past air pollution reductions in Europe. *Nature Geosci.*, 9, 277-281.

Kim, B. -M., S. -W. Son, S. -K. Min, J. -H. Jeong, S. -J. Kim, X. Zhang, T Shim, and J. -H. Yoon, 2014: Weakening of the stratospheric polar vortex by Arctic sea-ice loss. *Nat. Commun.*, 5, 4646, doi:10.1038/ncomms5646.

Lenaerts, J. T. M., K. Van Tricht, S. Lhermitte, and T. S. L'Ecuyer, 2017: Polar clouds and radiation in satellite observations, reanalyses and climate models. *Geophys. Res. Lett.*, 44, 3355-3364, doi: 10.1002/2016GL072242.

Makshtas, A. P., I. I. Bolshakova, R. M. Gun, O. L. Jukova, N. E. Ivanov, and S. V. Shutilin, 2011: Climate of the Hydrometeorological Observatory Tiksi region. In Meteorological and Geophysical Investigations. *Paulsen*, 2011, 49-74.

Notz, D., and J. Stroeve, 2016: Observed Arctic sea-ice loss directly follows anthropogenic CO_2 emission. *Science*, 354, 747-750, doi: 10.1126/science.aag2345.

Overland, J. E., 2009: The case for global warming in the Arctic. In: *Influence of Climate Change on the Changing Arctic and Sub-Arctic Conditions*, J. C. J. Nihoul and A. G. Kostianoy (eds.), Springer, 13-23.
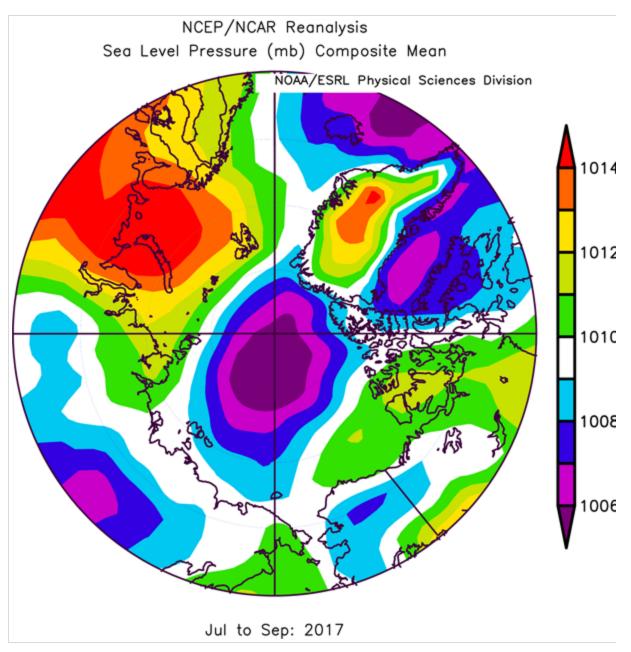
Overland, J. E., E. Hanna, I. Hanssen-Bauer, B. -M. Kim, S. -J. Kim, J. Walsh, M. Wang, and U. Bhatt, 2015: Air Temperature. In: *Arctic Report Card: Update for 2015*, ftp://ftp.oar.noaa.gov/arctic/documents/ArcticReportCard_full_report2015.pdf.

Overland, J. E., M. Wang, and T. J. Ballinger, 2017: Recent Increased Warming of the Alaskan Marine Arctic Due to Mid-latitude Linkages. *Adv. Atmos. Sci.*, 35, doi: 10.1007/s00376-017-7026-1.

Pithan, F., and T. Mauritsen, 2014: Arctic amplification dominated by temperature feedbacks in contemporary climate models. *Nature Geosci.*, 7, 181-184, doi: 10.1038/ngeo2071.

Serreze, M., and R. Barry, 2011: Processes and impacts of Arctic amplification: A research synthesis. *Global Planet. Change*, 77, 85-96.

November 30, 2017

Terrestrial Snow Cover

C. Derksen[1], R. Brown[1], L. Mudryk[1], K. Luojus[2], S. Helfrich[3]

[1]Climate Research Division, Environment and Climate Change Canada, Canada

[2]Arctic Research Centre, Finnish Meteorological Institute, Finland

[3]NOAA/NESDIS Center for Satellite Applications and Researc, USA

Highlights

- Spring snow cover extent (SCE) over Eurasia was above average in 2017, including the 2nd highest May SCE for Eurasia over the period of satellite observations (which date back to 1967). Consistent with below normal surface air temperatures in May and June, these are the first positive SCE anomalies observed in May over the Eurasian Arctic since 2005. June SCE anomalies were positive across the Eurasian Arctic for the first time since 2004.
- Greater than average April snow water equivalent (SWE) was present across Eurasia, a precursor to the above average snow extent later in the spring.
- SCE anomalies were once again below average (1981-2010 reference period) across the North American Arctic (11th time out of the past 12 years for May; 12th consecutive June) driven by earlier snow melt across the Canadian Arctic.

Satellite-derived estimates of SCE over Arctic land areas date back to 1967, and have shown dramatic reductions since 2005. This loss of spring snow over Arctic land areas is important because it influences the surface energy budget (snow is highly reflective of incoming solar energy), ground thermal regime (snow is a highly effective insulator of the underlying soil), and hydrological processes (the snowpack stores water in solid form for many months before spring melt). Current and projected changes in snow cover also generate a cascade of interactions and feedbacks that affect vegetation, biogeochemical activity, exchanges of carbon dioxide and trace gases, and ecosystem services (Brown et al., 2017). The spring (April, May, June) period is particularly important because the entire Arctic land area is snow covered during winter, so conditions during the melt season have a major impact on variability and trends in Arctic snow cover.

SCE anomalies (relative to the 1981-2010 reference period) for the Arctic (land areas north of 60N) in spring (April, May, June) 2017 were computed separately for the North American and Eurasian sectors of the Arctic. Anomalies were derived from the NOAA snow chart climate data record, which extends from 1967 to present (maintained at Rutgers University; Estilow et al., 2015; http://climate.rutgers.edu/snowcover/; **Fig. 1a-c**). For the first time in over a decade, Eurasian Arctic spring snow cover in 2017 was above average. April and May SCE anomalies were positive, including the 2nd highest May SCE in the period of satellite observations. These are the first positive SCE anomalies observed in May over the Eurasian Arctic since 2005, while June SCE anomalies were positive across the Eurasian Arctic for the first time since 2004. SCE anomalies over the North American Arctic were negative all spring, but did not approach the series of record-breaking low SCE values observed in recent years.

Fig. 1. Monthly snow cover extent (SCE) anomalies for Arctic land areas (>60° N) from the NOAA snow chart climate data record (CDR) for (a, left) April, (b, center) May and (c, right) June from 1967 to 2017. Anomalies are relative to the average for 1981-2010 and standardized (each observation differenced from the mean and divided by the standard deviation and thus unitless). Solid black and red lines depict 5-yr running means for North America and Eurasia, respectively.

Snow cover duration (SCD) departures, relative to a 1998-2010 reference period (used due to dataset availability) (**Fig. 2**) were derived from the NOAA daily Interactive Multisensor Snow and Ice Mapping System (IMS) snow cover product (Helfrich et al., 2007). While there was evidence of earlier snow cover onset over much of mid-latitude Eurasia (consistent with cold surface air temperature anomalies, see **Fig. 1.2a** in essay on *Surface Air Temperature*), the timing of snow onset over Arctic land areas (with the exception of parts of Alaska) was near normal. Later than normal snow melt onset across Eurasia (also reflected in the positive SCE anomalies in **Fig. 1**) was consistent with colder than normal surface air temperatures across this region (especially in May and June; see **Fig. 1.2c** in essay on *Surface Air Temperature*). In the North American Arctic, spring snow melt in the Canadian Arctic was slightly earlier than normal, coincident with warmer than average surface air temperatures in May and June (see **Fig. 1.2c** in essay on *Surface Air Temperature*).

Fig. 2. Snow cover duration (SCD in days) departures (difference from 1998-2010 mean) from the NOAA IMS data record for the 2016-2017 snow year: (a, left) autumn; and (b, right) spring.

Snow depth anomalies (**Fig. 3**) were derived from the Canadian Meteorological Centre (CMC) daily gridded global snow depth analysis, which combines surface observations with a simple snow model driven by temperature and precipitation forcing (Brasnett, 1999). In March and April, negative anomalies (i.e. relatively low snow depth) were observed across the subarctic, with mainly positive anomalies over the high latitude regions of Siberia and North America. Snow depth over the two continental sectors of the Arctic diverged by June; the Eurasian Arctic was characterized by extensive positive snow depth anomalies, while the North American Arctic was dominated by negative snow depth anomalies (which correspond to the region of shorter spring snow cover duration in **Fig. 2b**).

Fig. 3. Snow depth anomaly (% of the 1999-2010 average) in 2017 from the CMC snow depth analysis for (a, top left) March, (b, top right) April, (c, bottom left) May, and (d, bottom right) June.

Four products were utilized to generate a multi-dataset snow water equivalent (SWE; the amount of water stored in solid form as snow) anomaly time series (1980-2017) for April (typically the month of maximum SWE across the Arctic; **Fig. 4**). While compromising on time series length, the use of a multiple data sets tends to reduce uncertainty in the derived trends (for instance, see Brown and Derksen, 2013 and Mudryk et al., 2017 for issues related to the NOAA-CDR). The datasets used to derive the SWE time series included modern atmospheric reanalysis (The Modern-Era Retrospective Analysis for Research and Applications version 2; MERRA-2; Reichle et al., 2017), reconstructed snow cover driven by ERA-interim meteorology using the temperature-index model described by Brown et al. (2003), the physical snowpack model Crocus (Brun et al., 2013), and the European

Space Agency GlobSnow product derived using a combination of satellite passive microwave data and climate station observations (Takala et al., 2011). While there is a high degree of interannual variability in the multi-dataset SWE anomaly time series (calculated using the same 1981-2010 reference as **Fig. 1**), the anomalies have been predominantly negative since 2000. This was again the case for the North American Arctic in 2017. In contrast, Eurasian SWE anomalies were positive, which indicates a deeper than average snowpack was a precursor to the above average snow extent that followed later in the spring.

Fig. 4. Mean April SWE anomalies for Arctic land areas calculated from four independent products for North American (black) and Eurasian (red) sectors of the Arctic. Anomalies are relative to the average for 1981-2010 and standardized (each observation differenced from the mean and divided by the standard deviation and thus unitless). Solid black and red lines depict 5-yr running means for North America and Eurasia, respectively.

Even in the presence of a long term negative trend in Arctic spring SCE (driven by warming temperature trends), negative SCE anomalies are not expected in every season (nor in all regions) due to natural variability in the atmospheric circulation patterns which drive regional temperature and precipitation anomalies. The rebound in Eurasian SCE during May and June of 2017 was consistent with winter and spring season circulation patterns that

generally favored lower surface air temperatures, enhanced precipitation, and above-average snow accumulation across northern Eurasia (see essay on *Surface Air Temperature*).

References

Brasnett, B., 1999: A global analysis of snow depth for numerical weather prediction, *J. Appl. Meteorol.*, 38, 726-740.

Brown, R., B. Brasnett, and D. Robinson, 2003: Gridded North American monthly snow depth and snow water equivalent for GCM evaluation, *Atmos.-Ocean.*, 41, 1-14.

Brown, R., and C. Derksen. 2013. Is Eurasian October snow cover extent increasing? *Environ. Res. Lett.*, 8: 024006 doi: 10.1088/1748-9326/8/2/024006.

Brown, R., D. Vikhamar Schuler, O. Bulygina, C. Derksen, K. Luojus, L. Mudryk, L. Wang, and D. Yang, 2017: Arctic terrestrial snow cover, Chapter 3 in: *Snow, Water, Ice and Permafrost in the Arctic (SWIPA) 2017 Assessment*, Arctic Monitoring and Assessment Programme, Oslo, Norway.

Brun, E., V. Vionnet, A. Boone, B. Decharme, Y. Peings, R. Valette, F. Karbou, and S. Morin, 2013: Simulation of Northern Eurasian local snow depth, mass, and density using a detailed snowpack model and meteorological reanalyses, *J. Hydrometeorol.*, 14, 203-219, DOI: 10.1175/JHM-D-12-012.1.

Estilow, T. W., A. H. Young, and D. A. Robinson, 2015: A long-term Northern Hemisphere snow cover extent data record for climate studies and monitoring, *Earth Sys. Sci. Data*, 7.1, 137-142.

Helfrich, S., D. McNamara, B. Ramsay, T. Baldwin, and T. Kasheta, 2007: Enhancements to, and forthcoming developments in the Interactive Multisensor Snow and Ice Mapping System (IMS), *Hydrol. Process.*, 21, 1576-1586.

Mudryk, L., P. Kushner, C. Derksen, and C. Thackeray, 2017: Snow cover response to temperature in observational and climate model ensembles, *Geophys. Res. Lett.*, 44, DOI: 10.1002/2016GL071789.

Reichle, R., C. Draper, Q. Liu, M. Girotto, S. Mahanama, R. Koster, and G. De Lannoy, 2017: Assessment of MERRA-2 land surface hydrology estimates, *J. Clim.*, 30, DOI: 10.1175/JCLI-D-16-0720.1.

Takala, M., K. Luojus, J. Pulliainen, C. Derksen, J. Lemmetyinen, J. -P. Kärnä, and J. Koskinen, 2011: Estimating northern hemisphere snow water equivalent for climate research through assimilation of space-borne radiometer data and ground-based measurements, *Remote Sens. Environ.*, 115, 3517-3529.

November 20, 2017

Greenland Ice Sheet

M. Tedesco[1,2], J. E. Box[3], J. Cappelen[4], R. S. Fausto[3], X. Fettweis[5], K. Hansen[3], T. Mote[6], I. Sasgen[7], C. J. P. P. Smeets[8], D. van As[3], R. S. W. van de Wal[8], I. Velicogna[9]

[1]Lamont Doherty Earth Observatory of Columbia University, Palisades, NY, USA

[2]NASA Goddard Institute of Space Studies, New York, NY, USA

[3]Geological Survey of Denmark and Greenland, Copenhagen, Denmark

[4]Danish Meteorological Institute, Copenhagen, Denmark

[5]University of Liege, Liege, Belgium

[6]Department of Geography, University of Georgia, Athens, Georgia, USA

[7]Climate Sciences Department, Alfred Wegener Institute, Bremerhaven, Germany

[8]Institute for Marine and Atmospheric Research Utrecht, Utrecht University, Utrecht, The Netherlands

[9]Department of Earth System Science, University of California, Irvine, California, USA

Highlights

- The 2017 summer season over the Greenland ice sheet was characterized by below-average (1981-2010) melt extent and above-average surface albedo.
- The net 2017 ablation was below the 2008-2017 average at all ~20 PROMICE ablation area sites but still above the average for the 1961-1990 reference period, when the ice sheet was in steady equilibrium.
- The cumulative ice sheet mass balance up until April 2017 (end of GRACE observations) was close to the average of the years 2003-2016.
- Glacier area in 2017 continued a period of relative stability that started in 2012/2013.

Summary

Reflecting surface air temperature patterns over the Greenland ice sheet, the April 2016-April 2017 season was characterized by relatively low summer (June, July, August) melt extent and ablation along the margins of the ice sheet. Correspondingly, the surface albedo, averaged over the entire ice sheet, was relatively high. The net ice mass loss over the year was near average.

Surface Melting

The Greenland ice sheet is a major contributor to global sea level rise and plays a crucial role in the surface energy budget, climate and weather of the Arctic. Estimates of the spatial extent of melt across the Greenland ice sheet (GrIS) are obtained from brightness temperatures measured by the Special Sensor Microwave Imager/Sounder (SSMIS) passive microwave radiometer (e.g., Mote, 2007, Tedesco et al., 2013). These estimates show a rapid start to the 2017 melt season, similar to 2016, with melt extent in early April reaching an area typical of early June (**Fig. 1a**). From mid-June through mid-July, however, melt extent in 2017 was persistently below the 1981-2010 average, and below 2016 values over the same period. The spatial extent of melt for the period June, July and August (JJA) 2017 was above the average on 16% of summer days and reached its maximum extent of 32.9% of the ice sheet area on 26 July. This was low compared to the average maximum extent of 39.8% for the period 1981-2010, and was the lowest maximum extent since 1996. It is worth noting that on a more local scale, most of the western and northeast margins had more days than average with melt (relative to the 1981-2010 average), while the southeast margin had fewer days than average (**Fig. 1b**).
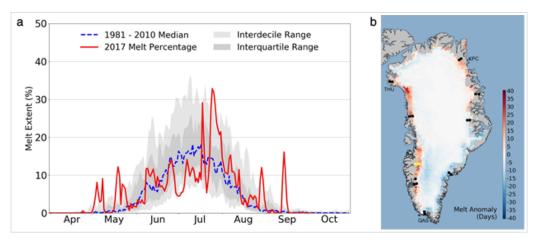
Fig. 1. a) Spatial extent of melt from SSMIS as a percentage of the ice sheet area during 2017 (red line) and the 1981-2010 mean spatial extent of melt (dashed blue line). The light and dark grey areas represent the interdecile and interquartile ranges, respectively. b) Map of the anomalies of the number of melting days obtained from passive microwave data for 2017, relative to the 1981-2010 mean. Black dots represent the locations of selected PROMICE stations and yellow squares show the location of the K-transect stations. Both plots were produced in conjunction with the National Snow and Ice Data Center.

The magnitude and evolution of surface melt in 2017 were consistent with the state of the Arctic Oscillation (AO) and North Atlantic Oscillation (NAO), both of which were strongly positive. When the AO or NAO are in a positive state, cyclonic conditions promote reduced incoming solar radiation and increased precipitation through increased cloudiness, for example, hence inhibiting melting and potentially promoting summer snowfall. These conditions are the opposite of those in 2012, when strong and persisting anti-cyclonic conditions promoted enhanced melting (e.g., Nghiem et al., 2012). Additionally, the 500 hPa geopotential heights across Greenland were persistently low across Greenland from June to mid-July 2017, a condition that is also typically associated with reduced melt extent. Late July and early August experienced positive geopotential height anomalies, and a negative NAO that promoted melting conditions across Greenland. As illustrated in **Fig. 1a**, this was a period of above average melt extent in summer 2017 (also see essay on *Surface Air Temperature*).

Surface Mass Balance

Consistent with low to moderate surface melting, the April 2016-April 2017 surface mass balance (SMB) year along the K-transect at 67° N in West Greenland (van de Wal et al., 2012) was characterized by moderate ice loss over the ablation region. **Figure 2a** shows the mass balance elevation profile of 2016-2017 together with the mean SMB elevation profile over the period 1990-2017. At most sites the SMB was approximately 1 standard deviation below average (1990-2017). Over the entire 27-year period there are only 4 years (1992, 1993, 1996, 2015) with less ablation along the transect (**Fig. 2b**). Overall, the distribution of the yearly-averaged mass balance over the transect is slightly positively skewed, with above average values over most of the later years except for the summers of 2015 and 2017. The equilibrium line altitude in 2017 was around 1490 meters, which is 40 m below the 27-year mean. The mass balance gradient was 3.4 mm w.e./m yr, which is about 6% lower than the average.

Fig. 2. a) Surface mass balance as a function of elevation along the K-transect for the period 2016-2017 and the mean over the period 1990-2017. The error bars are the standard deviation over the period 1990-2017; b) the distribution of the annually-averaged SMB at sites along the K-transect for the period 1990-2017, weighted according to the distance between sites (e.g., sites in the upper region are farther apart and given more weight); c) ablation anomalies for 2017 at lower ("L") PROMICE weather station sites in the Greenland ice sheet ablation area, referenced to the 1961-1990 period.

Net ablation in 2017 at 20 PROMICE sites, distributed around Greenland in the ablation zone, was at or below the average for the period of observations (2008-2017) at all locations. The most negative anomalies (< 1 SD below the 2008-2017 average) were found at the ice sheet margin at the TAS, NUK, UPE and THU sites. After referencing the values to the 1961-1990 climate-standard period and applying the Danish Meteorological Institute (DMI) air temperature scaling method of van As et al. (2016), only three of eight station sites at low elevation experienced ablation anomalies that were above average and beyond uncertainty in 2017: KPC_L (+96% ± 49%), SCO_L (+15% ± 14%) and KAN_L (+48% ± 35%) (**Fig. 2c**).

Total Mass Balance

GRACE satellite gravity estimates obtained following Velicogna et al. (2014) and Sasgen et al. (2012), available since 2002, indicate that between April 2016 and April 2017 (the most recent 12-month period of reliable data) there was a net ice mass loss of 276 ± 47 Gt (**Fig. 3**; 2-sigma uncertainty). The 2016-2017 net loss is greater than the April 2015-April 2016 mass loss (191 ± 28 Gt, see *Arctic Report Card 2016*) and close to the average April-to-April mass loss (255 ± 7 Gt) for 2003-2017 (Sasgen et al., 2012). The updated trends of total ice mass loss for the 15-year GRACE period are, respectively, 264 Gt/yr (Velicogna et al., 2014), and 270 Gt/yr (Sasgen et al., 2012).

Fig. 3. Change in the total mass (in Gigatonnes) of the Greenland ice sheet between April 2002 and June 2017, estimated from GRACE measurements following Velicogna et al. (2014, blue, CSR RL05) and Sasgen et al. (2012, red, GFZ RL05). Trends and correlation coefficients for the fitted linear trend are reported in the figure for the two estimates. Trends are corrected for glacial-isostatic adjustment using Simpson et al. 2009 applied to CSR RL05 and Khan et al. (2016) applied to GFZ RL05. Data between April 2002 and April 2017 are used here for trend analysis to be consistent with previous Arctic Report Cards.

Albedo

The area-averaged albedo for the entire Greenland ice sheet for summer 2017 (June through August, JJA) was 80.9%, using data from the Moderate-resolution Imaging Spectroradiometer (MODIS, after Box et al., 2017) (**Fig. 4a**). This is the 3rd highest JJA albedo value during the 2000-2017 MODIS period, after 2000 and 2013. High positive albedo anomalies are consistent with reduced melting in 2017 and snowfall events during the summer. For context, the minimum average summer albedo was recorded in 2012 (76.8%), the year of record maximum melt extent. High 2017 summer albedo anomalies occurred along the western margins of the ice sheet (**Fig. 4b**), where a strong albedo decrease associated with bare ice exposure and increased melting has been recently observed.

Surface Air Temperatures

Surface air temperatures observed on the ice sheet indicated a different pattern than those observed at coastal station, especially during summer 2017. Measurements at twenty coastal weather stations of the Danish Meteorological Institute (DMI) indicate widespread above- or near-average air temperatures for the seasons of autumn 2016 through summer 2017 (relative to the average for the period 1981-2010), with the exception of spring in northeast Greenland. New record highs were set at a number of sites in autumn 2016, with absolute anomalies above +5° C (see **Table 1**).

Table 1. Surface temperature anomalies [°C] and z-scores at a selection of the twenty DMI stations with a long record for the periods of autumn 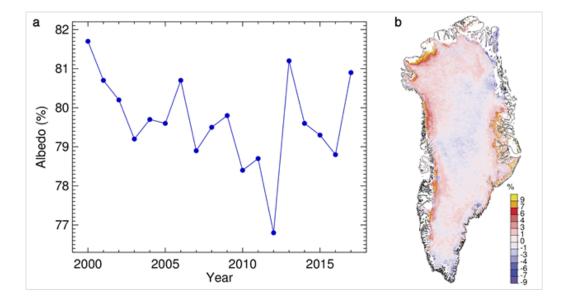2016 (SON), winter (DJF) 2017, spring (MAM) 2017 and summer (JJA) 2017. Station names, together with the year in which observations began and the corresponding coordinates are also reported, along with the years when maximum and minimum records were set. Bold text indicates the stations and periods when a new record was set.

Station Name, Start Year, Latitude, Longitude		SON 2016	DJF 16/17	MAM 2017	JJA 2017	Station Name, Start Year, Latitude, Longitude		SON 2016	DJF 16/17	MAM 2017	JJA 2017
Pituffik/Thule AFB 1948,76.5,68.8	Anomaly [°C]	0.4	0.5	0.2	-0.2	**Ivittuut/Narsarsuaq** 1873,61.2, 45.4	Anomaly [°C]	-0.1	1.4	1.3	0.2
	z-score	0.4	0.1	-0.1	-0.1		z-score	0.1	0.6	0.6	0.7
	Max Year	2010	1986	1953	1957		Max Year	2010	2010	2010	2016
	Min Year	1964	1949	1992	1996		Min Year	1874	1984	1989	1973
Station Nord 1961, 81.6, 16.7	Anomaly [°C]	4.4	2.7	-1.8	0.4	**Qaqortoq** 1807, 60.7,46.1	Anomaly [°C]	0.2	1.0	0.3	-0.1
	z-score	2.3	1.3	-0.8	0.5		z-score	0.6	0.6	0.0	0.1
	Max Year	**2016**	2011	2006	2003		Max Year	2010	2010	1932	1929
	Min Year	1989	1967	1961	1970		Min Year	1874	1863	1811	1811
Upernavik 1873, 72.8, 56.1	Anomaly [°C]	0.7	0.7	1.4	0.0	**Danmarkshavn** 1949,76.8, 18.7	Anomaly [°C]	5.3	0.6	-2.1	1.0
	z-score	0.7	0.3	0.5	0.6		z-score	3.3	0.4	-1.4	1.3
	Max Year	2010	1947	1932	2012		Max Year	**2016**	2005	1976	2016
	Min Year	1917	1983	1896	1873		Min Year	1971	1967	1966	1955
Kangerlussuaq 1949, 67.0, 50.7	Anomaly [°C]	0.2	-0.7	-0.4	0.3	**Illoqqortoormiut** 1949,70.5,22.0	Anomaly [°C]	4.2	2.5	-0.9	0.2
	z-score	0.1	-0.4	-0.2	0.0		z-score	2.7	1.2	0.1	0.8
	Max Year	2010	1986	2016	1960		Max Year	**2016**	2014	1996	2016
	Min Year	1982	1983	1993	1983		Min Year	1951	1966	1956	1955
Ilulissat 1807, 69.2, 51.1	Anomaly [°C]	-0.2	0.1	0.1	-0.5	**Tasiilaq** 1895, 65.6, 37.6	Anomaly [°C]	2.3	2.3	1.3	0.2
	z-score	0.3	0.3	0.1	0.3		z-score	2.2	1.4	0.8	0.0
	Max Year	2010	1929	1847	1960		Max Year	1941	1929	1929	2016
	Min Year	1837	1863	1813	1863		Min Year	1917	1918	1899	1983
Aasiaat 1958, 68.7, 52.8	Anomaly [°C]	0.5	0.8	0.6	0.3	**Prins Christian Sund** 1958, 60.1,42.2	Anomaly [°C]	1.3	0.6	0.2	-0.2
	z-score	0.6	0.0	0.2	0.3		z-score	1.5	0.4	0.3	-0.2
	Max Year	2010	2010	2016	2012		Max Year	2010	2010	2005	2010

	Min Year	1986	1984	1993	1972		Min Year	1982	1993	1989	1970

Nuuk 1784, 64.2, 51.7	Min Year	1986	1984	1993	1972	**Summit** 1991, 72.6, 38.5	Min Year	1982	1993	1989	1970
	Anomaly [°C]	-0.2	0.6	0.1	0.2		Anomaly [°C]	2.2	1.4	0.6	-0.6
	z-score	0.2	0.4	0.0	0.3		z-score	1.1	0.7	0.3	-0.6
	Max Year	2010	2010	1932	2012		Max Year	2002	2010	2016	2012
	Min Year	1811	1818	1802	1819		Min Year	2009	1993	1992	1992
Paamiut 1958,62.0,49.7	Anomaly [°C]	0.4	1.3	-0.2	0.0						
	z-score	0.3	0.3	-0.2	0.0						
	Max Year	2010	2010	2005	2010						
	Min Year	1982	1984	1993	1969						

Consistent with surface mass balance observations, July 2017 was the coldest in the 2008-2017 period along the western ice sheet ablation area at the PROMICE sites. Summer (JJA) temperatures were at or below the 2008-2017 average at all stations, and by more than one standard deviation below the average along the entire western slope, consistent with in average or below average ablation. Out of all January-August 2017 station-months, 21% were colder than one standard deviation below average, and only 2% were over one standard deviation above average temperature. At Greenland's Summit Station, a record low July temperature of -33.0° C was measured on July 4 (previous record: -30.7° C), and a record high July temperature of +1.9° C was measured on July 28 (previous record: +0.8° C).

Marine-Terminating Glaciers

Marine-terminating glaciers are the outlets via which the Greenland ice sheet discharges ice mass to the ocean. Glacier area measurements from LANDSAT and ASTER imagery available since 1999 (Box and Hansen, 2015) for fifteen of the widest and fastest-flowing marine-terminating glaciers reveal a pattern of continued relative stability that started in 2012/2013. The annual net area change at the end of the melt season in September 2017 was -13.5 km^2, which is below the 18-year survey period average of -59.9 km^2 per year. Among the fifteen surveyed glaciers, seven retreated, five were stable and three advanced. The largest area losses were in eastern Greenland, with the Helheim and Kangerdlugssauq glaciers losing, respectively, 11.6 km^2 and 9.9 km^2 in area. The largest advance was observed at Petermann glacier, in the northwest, with a change of +11.5 km^2.

Acknowledgments

References

Box, J. E., and K. Hansen, 2015: Survey of Greenland glacier area changes. PROMICE newsletter 8, December 2015, http://promice.org/Newsletter_08.pdf.

Box, J. E., D. van As, and K. Steffen, 2017: Greenland, Canadian and Icelandic land ice albedo grids (2000-2016). *Geological Survey of Denmark and Greenland Bulletin*, 38, 53-56.

Khan, S. A., I. Sasgen, M. Bevis, T. van Dam, J. L. Bamber, J. Wahr, M. Willis, K. H. Kjær, B. Wouters, V. Helm, and B. Csatho, 2016: Geodetic measurements reveal similarities between post-Last Glacial Maximum and present-day mass loss from the Greenland ice sheet. *Science Advances*, 2(9), e1600931.

Mote, T., 2007: Greenland surface melt trends 1973-2007: Evidence of a large increase in 2007. *Geophysical Research Letters*, 34, L22507.

Nghiem, S. V., D. K. Hall, T. L. Mote, M. Tedesco, M. R. Albert, K. Keegan, C. A. Shuman, N. E. DiGirolamo, and G. Neumann, 2012: The extreme melt across the Greenland ice sheet in 2012. *Geophysical Research Letters*, 39, L20502, doi: 10.1029/2012GL053611.

Sasgen, I., M. van den Broeke, J. L. Bamber, E. Rignot, L. S. Sørensen, B. Wouters, Z. Martinec, I. Velicogna, I., and S. B. Simonsen, 2012: Timing and origin of recent regional ice-mass loss in Greenland. *Earth and Planetary Science Letters*, 333, 293-303.

Simpson, M. J. R., G. A. Milne, P. Huybrechts, and A. J. Long, 2009: Calibrating a glaciological model of the Greenland ice sheet from the Last Glacial Maximum to present-day using field observations of relative sea level and ice extent. *Quaternary Science Reviews*, 28(17-18), 1631–1657.

Tedesco, M., X. Fettweis, T. Mote, J. Wahr, P. Alexander, J. Box, and B. Wouters, 2013: Evidence and analysis of 2012 Greenland records from spaceborne observations, a regional climate model and reanalysis data. *The Cryosphere*, 7, 615-630.

van As, D., R. S. Fausto, J. Cappelen, R. S. W. van de Wal, R. J. Braithwaite, H. Machguth, and PROMICE project team, 2016: Placing Greenland ice sheet ablation measurements in a multi-decadal context. *Geological Survey of Denmark and Greenland Bulletin*, 35, 71-74.

van de Wal, R. S. W., W. Boot, C. J. P. P. Smeets, H Snellen, M. R. van den Broeke, and J. Oerlemans, 2012: Twenty-one years of mass balance observations along the K-transect, West-Greenland. *Earth System Science Data*, 4, 31-35, doi: 10.5194/essd-4-31-2012.

Velicogna, I., T. C. Sutterley, and M. R. van den Broeke, 2014: Regional acceleration in ice mass loss from Greenland and Antarctica using GRACE time-variable gravity data. *Geophysical Research Letters*, 41, 8130–8137, doi: 10.1002/2014GL061052.

December 6, 2017

Sea Ice

D. Perovich[1], W. Meier[2], M. Tschudi[3], S. Farrell[4], S. Hendricks[5], S. Gerland[6], C. Haas[5], T. Krumpen[5], C. Polashenski[1,7], R. Ricker[5], M. Webster[8]

[1]Thayer School of Engineering, Dartmouth College, Hanover, NH, USA

[2]National Snow and Ice Data Center, Boulder, CO, USA

[3]Aerospace Engineering Sciences, University of Colorado, Boulder, CO, USA

[4]NOAA Earth System Science Interdisciplinary Center, University of Maryland, College Park, MD, USA

[5]Alfred Wegener Institute, Helmholtz Centre for Polar and Marine Research, Bremerhaven, Germany

[6]Norwegian Polar Institute, Fram Centre, Tromsø, Norway

[7]ERDC - CRREL, 72 Lyme Road, Hanover, NH, USA

[8]NASA Goddard Space Flight Center, Greenbelt, MD, USA

Highlights

- The lowest winter maximum ice extent in the satellite record (1979-2017) occurred on 7 March 2017. The extent was 14.42 million km^2, 8% below the 1981-2010 average. This was the third straight year of a record low winter maximum.
- The September 2017 Arctic sea ice minimum extent was 4.64 million km^2, 25% lower than the 1981-2010 average minimum ice extent and the eighth lowest value in the satellite record (1979-2017). The ten lowest September extents have occurred in the last 11 years.
- In March 2017, multiyear ice (more than 1 year old) and first-year ice were 21% and 79% of the ice cover, respectively, compared to 45% and 55% in 1985 (start of record).
- CryoSat-2 results showed the third lowest central Arctic Ocean sea ice volume in April 2017 of the satellite's data record (2011-2017), after April 2012 and April 2013.
- There has been an overall decrease in end of winter snow depth on the sea ice cover in the western Arctic in the past decade.

Sea Ice Extent

The Arctic sea ice cover varies substantially over the year, with end-of-winter ice cover generally two to three times as large as at the end of summer. Sea ice is an important element of the climate system: (1) acting as a barrier between the underlying ocean and the atmosphere, (2) limiting the amount of absorbed solar energy due to its high albedo, (3) providing a habitat for biological activity, and (4) limiting human access to the Arctic Ocean. Sea ice extent (designated by a 15% sea ice concentration threshold) has been monitored using passive microwave instruments on satellite platforms since 1979. The months of September and March are of particular interest because they are the months when the Arctic sea ice typically reaches its minimum and maximum extents, respectively. **Figure 1** shows maps of monthly average ice extents in March 2017 and September 2017.

Fig. 1. Average monthly sea ice extent in March 2017 (left) and September 2017 (right) illustrate the respective winter maximum and summer minimum extents. The magenta line indicates the median ice extents in March and September, respectively, during the period 1981-2010. Maps are from NSIDC at nsidc.org/data/seaice_index (Fetterer et al., 2002).

Based on estimates produced by the National Snow and Ice Data Center (NSIDC) Sea Ice Index (Fetterer et al., 2002), the sea ice cover reached a maximum extent of 14.42 million km^2 on March 7, 2017. This was 8% below the 1981-2010 average. For the third straight year, the Arctic sea ice has experienced a new record lowest maximum value in the satellite record. The maximum extent occurred 5 days earlier than the 1981-2010 average (12 March).

On September 13, 2017, the sea ice cover reached a summer minimum value of 4.64 million km^2. This was the eighth lowest extent of the satellite record. While it represents a modest increase from the 2016 minimum, it was 25% less than the 1981-2010 median minimum ice extent. The ten lowest September extents have occurred in the last 11 years (Parkinson and DiGirolamo, 2016). The September ice extent has not returned to pre-2007 levels.

Sea ice extent has decreasing trends in all months and virtually all regions except for the Bering Sea during winter (Meier et al., 2014). The September monthly average trend for the entire Arctic Ocean is now -13.2% per decade

relative to the 1981-2010 average (**Fig. 2**). Trends are smaller during March (-2.7% per decade), but the decrease is statistically significant.

Fig. 2. Time series of ice extent anomalies in March (the month of maximum ice extent) and September (the month of minimum ice extent). The anomaly value for each year is the difference (in %) in ice extent relative to the mean values for the period 1981-2010. The black and red dashed lines are least squares linear regression lines. The slopes of these lines indicate ice losses of -2.7% and -13.2% per decade in March and September, respectively. Both trends are significant at the 99% confidence level.

Age of the Ice

The age of sea ice is another key descriptor of the state of the sea ice cover. It serves as an indicator for ice physical properties, including thickness, surface roughness, and melt pond coverage (Tschudi et al., 2016). Compared to younger ice, older ice tends to be thicker, stronger and more resilient to changes in atmospheric and oceanic forcing. The age of the ice is determined using satellite observations and drifting buoy records to track ice parcels over several years (Tschudi et al., 2010; Maslanik et al., 2011). This method has been used to provide a record of the age of the ice from 1985 to the present (Tschudi et al., 2015).

Very old ice (>4 years old) continues to make up a small fraction of the Arctic ice pack in March, when the sea ice extent is at its maximum (**Fig. 3**). In 1985, 16% of the ice pack was very old ice, but by March 2017, this ice category only constituted 0.9% of the ice pack. The extent of the oldest ice declined from 2.54 million km^2 in March 1985 to 0.13 million km^2 in March 2017. The distribution of ice age in March 2017 was similar to that in March of the previous year, although there was a decrease in the oldest ice fractional coverage, from 1.2% in March 2016 to 0.9% in March 2017.

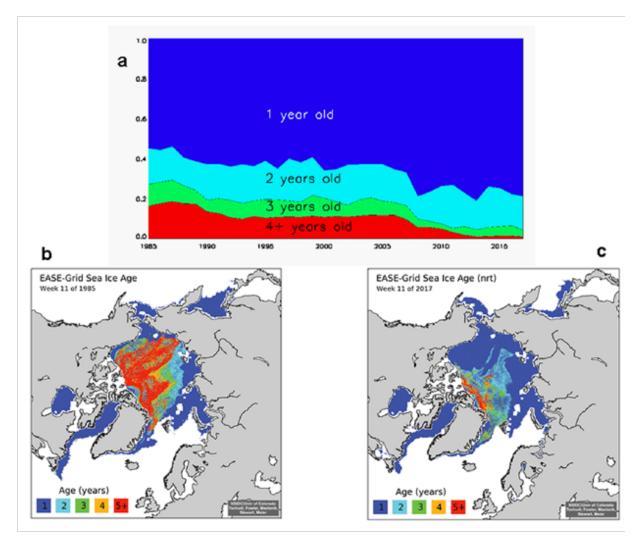Fig. 3. (a) Sea ice age coverage by year, 1985-2017. Sea ice age coverage maps for (b) March 1985 and (c) March 2017.

First-year ice now dominates the winter sea ice cover, comprising ~79% of the ice cover in March 2017, compared to about 55% in the 1980s. The thinner, younger ice is more vulnerable to completely melting in the summer, resulting in lower minimum ice extents.

Sea Ice Thickness

Satellite remote sensing and regular airborne survey programs continued to record changes in Arctic sea-ice thickness and volume. In 2017, the ESA CryoSat-2 radar altimeter mission completed its 7th year of operation since its launch in 2010, providing sea-ice thickness between October and April (Laxon et al., 2013) from freeboard observations. The CryoSat-2 freeboard measurements expand the data record of satellite and submarine based observations that document the decline in sea-ice thickness in the last decades (Kwok and Rothrock, 2009; Lindsay and Schweiger, 2015).

In spring 2017, CryoSat-2 products from the Alfred Wegener Institute (AWI) indicated a pattern of ice thickness change that was more variable (**Fig. 4a**) compared to previous years (2011-2016) in the observational period (**Fig. 4b**). The April 2017 thickness anomaly (**Fig. 4c**) shows below average thicknesses in the multiyear ice region north of the Canadian Archipelago, the Chukchi Sea and the shelf regions of the East Siberian Sea. Above-average thicknesses were observed in the Beaufort Sea and the eastern part of the central Arctic Ocean. The magnitude of these anomalies was generally below 1 meter.

Fig. 4. (a) Sea-ice thickness from CryoSat-2 radar altimeter data for April 2017, (b) mean April data record, for the period 2011-2016, and (c) the April 2017 sea-ice thickness anomaly. (Data source: AWI CryoSat sea ice product, www.seaiceportal.de)

The CryoSat-2 sea-ice volume estimates (**Fig. 5**) for the central Arctic Ocean showed a continued decline from 2014 through 2017. The April 2017 sea-ice volume of 13.19 ± 1.15 thousand cubic kilometers ranks as the third lowest spring volume after April 2012 (13.14 ±1.27) and 2013 (12.56 ± 1.21) in the AWI CryoSat-2 data record. The difference between the three lowest volume estimates lies within the observational uncertainties.

Fig. 5. (a) Monthly time series of sea ice volume from CryoSat-2 measurements for the months November (minimum volume) to April (maximum volume). Number in the markers indicate the ranking of each month for the seven years of the data record, with 1 representing the smallest volume and 7 the largest. (b) The shaded area denotes the region where ice volume was determined.

Snow on Sea Ice

Snow plays several critical roles in the mass balance of Arctic sea ice. During the winter growth season, snow insulates the ocean from the atmosphere, dampening heat fluxes and reducing sea ice growth. In spring, snow reflects more than 80% of the incoming solar radiation, delaying ice melt. Snow can also contribute to ice growth after flooding and refreezing, leading to formation of snow ice (Granskog et al., 2017). As the melt season progresses, freshwater from snowmelt enables the formation of ponds on the sea ice.

Prior to the 1990s, observations of snow on Arctic sea ice were limited to in situ measurements. Warren et al. (1999) compiled many of these observations into a climatology. Since the 1990s, new approaches to measure snow accumulation have rapid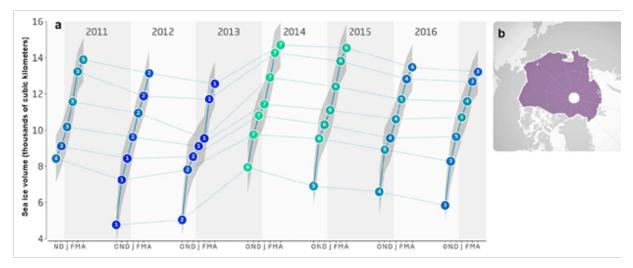ly emerged, including improved instruments for in situ and autonomous observations and remote sensing techniques for retrieving snow depth. Field observations from recent years continue to underscore significant regional and inter-annual variability in Arctic snow on sea ice conditions. **Figure 6** shows the historical snow depth climatology (background) plus a compilation of recent airborne snow depth measurements collected between March and May in 2009-2012 and 2014-2015 (lines), and in situ measurements made in 2015 and 2017 (individual points). Mean snow depths range from ~0.05 m to 0.55 m as shown. Compared to the climatology, these data indicate that there has been an overall decrease in snow depths in the western Arctic at the end of winter, potentially associated with later sea ice formation in the autumn and the shift from MY to FY ice. (Webster et al., 2014). Airborne observations confirm that snow on first year ice is thinner than that on multi-year ice (Kurtz and Farrell, 2011; Blanchard-Wrigglesworth et al., 2015).

Fig. 6. Snow depth on Arctic sea ice at the end of winter, prior to melt onset. Recent in situ measurements (stars) at a variety of field sites, as well as airborne observations (dots along multiple flight survey lines) are overlaid on the climatological mean snow depth for the months of March and April (adapted from Warren et al., 1999).

References

Blanchard-Wrigglesworth, E., S. L. Farrell, T. Newman, and C. M. Bitz, 2015: Snow cover on Arctic sea ice in observations and an Earth System Model. *Geophys. Res. Lett.*, doi: 10.1002/2015GL066049.

Fetterer, F., K. Knowles, W. Meier, and M. Savoie, 2002, updated daily: Sea Ice Index. Boulder, Colorado USA: National Snow and Ice Data Center. http://dx.doi.org/10.7265/N5QJ7F7W.

Granskog, M. A., A. Rösel, P. A. Dodd, D. Divine, S. Gerland, T. Martma, and M. J. Leng, 2017: Snow contribution to first-year and second-year Arctic sea ice mass balance north of Svalbard. *J. Geophys. Res.-Oceans*, 22, doi:

10.1002/2016JC012398.

Kurtz, N. T., and S. L. Farrell, 2011: Large-scale surveys of snow depth on Arctic sea ice from Operation IceBridge. *Geophys. Res. Lett.*, 38, L20505, doi: 10.1029/2011GL049216.

Kwok, R., and D. A. Rothrock, 2009: Decline in Arctic sea ice thickness from submarine and ICESat records: 1958-2008. *Geophys. Res. Lett.*, 36, doi: 10.1029/2009GL039035.

Laxon, S. W., K. A. Giles, A. L. Ridout, D. J. Wingham, R. Willatt, R. Cullen, R. Kwok, A. Schweiger, J. Zhang, C. Haas, S. Hendricks, R. Krishfield, N. Kurtz, S. Farrell, and M. Davidson, 2013: CryoSat-2 estimates of Arctic sea ice thickness and volume. *Geophys. Res. Lett.*, 40, 732-737, doi: 10.1002/grl.50193.

Lindsay, R., and A. Schweiger, 2015: Arctic sea ice thickness loss determined using subsurface, aircraft, and satellite observations. *The Cryosphere*, 9, 269-283.

Maslanik, J., J. Stroeve, C. Fowler, and W. Emery, 2011: Distribution and trends in Arctic sea ice age through spring 2011. *Geophys. Res. Lett.*, 38, doi: 10.1029/2011GL047735.

Meier, W. N., G. Hovelsrud, B. van Oort, J. Key, K. Kovacs, C. Michel, M. Granskog, S. Gerland, D. Perovich, A. P. Makshtas, and J. Reist, 2014: Arctic sea ice in transformation: A review of recent observed changes and impacts on biology and human activity. *Rev. Geophys.*, 41, doi: 10.1002/2013RG000431.

Parkinson, C., and N. DiGirolamo, 2016: New visualizations highlight new information on the contrasting Arctic and antarctic sea-ice trends since the late 1970s. *Rem. Sens. Envir.*, 183, 198-204, doi.org/10.1016/j.rse.2016.05.020.

Tschudi, M. A., C. Fowler, J. A. Maslanik, and J. A. Stroeve, 2010: Tracking the movement and changing surface characteristics of Arctic sea ice. *IEEE J. Sel. Topics Earth Obs. and Rem. Sens.*, 3, doi: 10.1109/JSTARS.2010.2048305.

Tschudi, M., C. Fowler, and J. Maslanik, 2015: EASE-Grid Sea Ice Age, Version 2. Boulder, Colorado USA. *NASA National Snow and Ice Data Center Distributed Active Archive Center*, doi: 10.5067/1UQJWCYPVX61.

Tschudi, M. A., J. C. Stroeve, and J. Scott Stewart (2016), Relating the age of Arctic sea ice to its thickness, as measured during NASA's ICESat and IceBridge Campaigns. *Remote Sens.*, 8(6), 457; doi: 10.3390/rs8060457.

Warren, S., I. Rigor, N. Untersteiner, V. F. Radionov, N. N. Bryazgin, Y. I. Aleksandrov, and R. Colony, 1999: Snow depth on Arctic sea ice. *J. Clim.*, 12, 1814-1829.

Webster, M. A., I. G. Rigor, S. V. Nghiem, N. T. Kurtz, S. L. Farrell, D. K. Perovich, and M. Sturm, 2014: Interdecadal changes in snow depth on Arctic sea ice. *J. Geophys. Res.-Oceans*, 119, 5395-5406, doi: 10.1002/2014JC009985.

November 30, 2017

Sea Surface Temperature

M. -L. Timmermans[1], C. Ladd[2], K. Wood[2]

[1]Yale University, New Haven, CT, USA

[2]Pacific Marine Environmental Laboratory, NOAA, Seattle, WA, USA

Highlights

- Sea surface temperatures (SSTs) in August 2017 were up to +4° C warmer than the 1982-2010 August mean in regions of the Barents and Chukchi seas.
- In the Arctic Basin, spatial patterns of August 2017 SST anomalies relative to the 1982-2010 August mean are linked to regional variability in sea-ice retreat, regional air temperature, and advection of waters from the Pacific and Atlantic oceans.
- The Chukchi Sea shows an ocean surface warming trend over 1982-2017 of ~0.7° C/decade.

Summer sea surface temperatures (SST) in the Arctic Ocean are set mainly by absorption of solar radiation into the surface layer. In the Barents and Chukchi seas, there is an additional contribution from advection of warm water from the North Atlantic and Pacific oceans, respectively. Solar warming of the ocean surface layer is influenced by the distribution of sea ice (with more solar warming in ice-free regions), cloud cover, water color, and upper-ocean stratification. River influxes influence the latter two, as well as provide an additional source of warm water. SSTs are an essential indicator of the role of the ice-albedo feedback mechanism in any given melt season: as the area of ice cover decreases, more incoming solar radiation is absorbed by the ocean and the warmer ocean in turn melts more sea ice. SST data presented here are from the NOAA Optimum Interpolation (OI) SST Version 2 product (OISSTv2), which is a blend of in situ and satellite measurements (Reynolds et al., 2002, 2007). Compared to in situ temperature measurements, the OISSTv2 product showed average correlations of about 80%, with an overall cold SST bias of -0.02° C (Stroh et al., 2015).

August SSTs provide the most appropriate representation of Arctic Ocean summer SSTs because they are not affected by the cooling and subsequent sea-ice growth that typically takes place in the latter half of September. Mean SSTs in August 2017 in ice-free regions ranged from ~0° C in some regions to as high as +11° C in the Chukchi and Barents seas (**Fig. 1a**). Compared to the 1982-2010 August mean (note the monthly SST record begins in December 1981), most boundary regions and marginal seas had anomalously warm SSTs in August 2017 (**Fig. 1b**). Particularly warm anomalies (around 3-4° C warmer than the 1982-2010 average) were observed in the Beaufort, Chukchi and southern Barents seas. SSTs in the boundary regions and marginal seas, which are mostly ice free in August, are linked to the timing of local sea ice retreat, which facilitates the direct solar heating of the exposed surface waters.

Fig. 1. (a) Mean SST (°C) in Aug 2017. White shading is the Aug 2017 mean sea ice extent, and gray contours indicate the 10° C SST isotherm. (b) SST anomalies (°C) in Aug 2017 relative to the Aug 1982-2010 mean (the dotted black contour indicates zero anomaly). White shading is the Aug 2017 mean ice extent and the black line indicates the median ice edge for Aug 1982 2010 mean. (Sources: SST data are from the NOAA OISSTv2; sea ice extent and ice-edge data are from NSIDC.)

In August 2017, regions off the west and east coasts of Greenland and in the southern Barents Sea were markedly cooler (by up to 3° C) than in August 2016 (**Fig. 2a**). It is notable also that compared to August 2012 (the summer of lowest minimum sea-ice extent in the satellite record, 1979-present) August SSTs in the Chukchi Sea region were up to 3° C warmer in 2017 (**Fig. 2b**). This illustrates the significant interannual and spatial variability in summer SSTs. Colder conditions in August 2012 (compared to August 2017) in the Chukchi Sea were related to the persistence of sea ice in that particular region (even while the main ice pack retreated) and a strong cyclonic

storm in the region that occurred late in the summer season, during the first week of August (see Timmermans et al., 2013).

Fig. 2. SST anomalies (°C) in Aug 2017 relative to (a) Aug 2016 and (b) Aug 2012. White shading is the Aug 2017 mean ice extent and the black line indicates the median ice edge for (a) Aug 2016 and (b) Aug 2012.

Mean August SSTs from 1982-2017 show statistically significant linear warming trends over much of the Arctic Ocean (**Fig. 3a**); the cooling trends in the Laptev and northern Barents seas are notable exceptions. Mean August SSTs for the entire Chukchi Sea region exhibit a statistically significant warming trend over the duration of the record; August SSTs in this region are warming at a rate of about +0.7° C decade^{-1}, based on a linear fit (**Fig. 3b**). Warming trends coincide with declining trends in summer sea-ice extent (including late-season freeze-up and early melt, e.g., Parkinson, 2014), increased solar absorption (e.g., Pinker et al., 2014), release of stored ocean heat (e.g., Timmermans et al., 2015), and milder air temperatures (see essay on *Surface Air Temperature*).

Fig. 3. (a) Linear SST trend (°C yr^{-1}) for Aug of each year from 1982-2017. The trend is only shown for values that are significant at the 95% confidence interval; the region is grey otherwise. White shading is the Aug 2017 mean ice extent and th black line indicates the median ice edge for Aug 1982-2010 mean. (b) Area-averaged SST anomalies (°C) for Aug of each yea relative to the 1982-2010 Aug mean for the Chukchi Sea region shown by the dotted lines in (a). The dashed black line shows the linear SST trend (over the period shown) for the Chukchi Sea, with 95% confidence interval.

References

Parkinson, C. L., 2014: Spatially mapped reductions in the length of the Arctic sea ice season. *Geophys. Res. Lett.*, 41, 4316-4322, doi: 10.1002/2014GL060434.

Pinker, R. T., X. Niu, and Y. Ma, 2014: Solar heating of the Arctic Ocean in the context of ice-albedo feedback. *J. Geophys. Res. Oceans*, 119, 8395-8409, doi: 10.1002/2014JC010232.

Reynolds, R. W., N. A. Rayner, T. M. Smith, D. C. Stokes, and W. Wang, 2002: An improved in situ and satellite SST analysis for climate. *J. Climate*, 15, 1609-1625.

Reynolds, R. W., T. M. Smith, C. Liu, D. B. Chelton, K. S. Casey, and M. G. Schlax, 2007: Daily high-resolution-blended analyses for sea surface temperature. *J. Climate*, 20, 5473-5496, and see http://www.esrl.noaa.gov/psd/data/gridded/data.noaa.oisst.v2.html.

Stroh, J. N., G. Panteleev, S. Kirillov, M. Makhotin, and N. Shakhova, 2015: Sea-surface temperature and salinity product comparison against external in situ data in the Arctic Ocean. *J. Geophys. Res. Oceans*, 120, 7223-7236, doi: 10.1002/2015JC011005.

Timmermans, M. -L., I. Ashik, Y. Cao, I. Frolov, R. Ingvaldsen, T. Kikuchi, R. Krishfield, H. Loeng, S. Nishino, R. Pickart, B. Rabe, I. Semiletov, U. Schauer, P. Schlosser, N. Shakhova, W. M. Smethie, V. Sokolov, M. Steele, J. Su, J. Toole, W. Williams, R. Woodgate, J. Zhao, W. Zhong, and S. Zimmermann, 2013: [The Arctic] Ocean Temperature and Salinity [in "State of the Climate in 2012"]. *Bull. Amer. Meteor. Soc.*, 94(8), S128-S130.

Timmermans, M. -L., 2015: The impact of stored solar heat on Arctic sea-ice growth. *Geophys. Res. Lett.*, 42, doi: 10.1002/2015GL064541.

Timmermans, M. -L., 2017: [The Arctic] Sea Surface Temperature [in "State of the Climate in 2016"]. *Bull. Amer. Meteor. Soc.*, 98 (8), S135-S136.

November 20, 2017

Arctic Ocean Primary Productivity

K. E. Frey[1], J. C. Comiso[2], L. W. Cooper[3], L. B. Eisner[4],
R. R. Gradinger[5], J. M. Grebmeier[3], J. -É. Tremblay[6]

[1]Graduate School of Geography, Clark University, Worcester, MA, USA

[2]Cryospheric Sciences Laboratory, NASA Goddard Space Flight Center, Greenbelt, MD, USA

[3]Chesapeake Biological Laboratory, University of Maryland Center for Environmental Science, Solomons, MD, USA

[4]Alaska Fisheries Science Center, NOAA, Seattle, WA, USA

[5]UiT, The Arctic University of Norway, Tromsø, Norway

[6]Québec-Océan and Takuvik, Biology Department, Université Laval, Québec City, QC, Canada

Highlights

- Estimates of ocean primary productivity via satellite observations showed widespread positive (increasing) anomalies for 2017 (relative to the 2003-2016 mean) for all regions, with the most pronounced overall trends over the years 2003-2017 occurring in the Barents Sea and Eurasian Arctic regions.
- The regional distribution of positive (negative) anomalies in chlorophyll-*a* concentrations can often be associated with a relatively early (late) breakup of the sea ice cover.
- During May 2017, strong positive anomalies in chlorophyll-*a* concentrations occurred in the northwestern Bering Sea and in the southeastern Chukchi Sea off the coast of Point Hope, while widespread negative anomalies occurred in the Barents Sea. Negative anomalies for 2017 were also prevalent across broad areas of the Kara and Laptev seas, particularly during June, July, and August.
- Some of the most significant increases in chlorophyll-*a* concentrations over the years 2003-2017 have occurred during May in localized areas of the Labrador Sea and the Barents Sea.

Introduction

Autotrophic minute algae living in the sea ice (ice algae) and water column (phytoplankton) are the main primary producers in the Arctic Ocean. Through photosynthesis, they transform dissolved inorganic carbon dioxide into organic material. Consequently, primary production provides a key ecosystem service by providing energy to the entire food web in the oceans. The global oceans play a significant role in global carbon budgets via photosynthesis, contributing approximately half of Earth's net annual photosynthesis with ~10-15% of this production occurring on the continental shelves alone (Müller-Karger et al., 2005). Primary productivity is strongly dependent upon light availability and the presence of nutrients, and thus is highly seasonal in the Arctic region. In particular, the melting and retreat of sea ice during spring are strong drivers of primary production in the Arctic Ocean and its adjacent shelf seas due to enhanced light availability and stratification (Barber et al., 2015; Leu et al., 2015; Ardyna et al., 2017). Recent declines in Arctic sea ice extent (see the essay on *Sea Ice*) have contributed substantially to shifts in primary productivity throughout the Arctic Ocean. However, the response of primary production to sea ice loss has been both seasonally and spatially variable (e.g., Tremblay et al., 2015; Hill et al., 2017).

Here we present satellite-based estimates of algal chlorophyll-*a* (occurring in all species of phytoplankton), based on the color of the ocean, and subsequently provide calculated primary production estimates. These results are shown for ocean areas with less than 15% sea ice concentration and, therefore, do not include production by sea ice algae, open water from within the sea ice pack, or under-ice phytoplankton blooms.

Chlorophyll-*a*

Measurements of the algal pigment chlorophyll (e.g., chlorophyll-*a*) serve as a proxy for the amount of algal biomass present as well as overall plant health. Here we present the complete, updated MODIS-Aqua satellite chlorophyll-*a* record for the northern polar region for the years 2003-2017. A base period of 2003-2016 is chosen to calculate the 2017 anomalies to maximize the length of the short satellite-based time series.

The 2017 data show a distribution of both positive and negative anomalies in chlorophyll-*a* concentrations in a number of locations across the Arctic Ocean region, where patterns are spatially and temporally heterogeneous (**Fig. 1**). These patterns are often associated with the timing of sea ice breakup: positive anomalies tend to occur in regions where the breakup is relatively early, while negative anomalies tend to occur in regions where the breakup is delayed. The most notable positive anomaly in 2017 occurred during May, with high concentrations of chlorophyll-*a* (averaging over ~12 mg m^{-3} higher than the 2003-2016 mean) occurring across a relatively large (~500 x 350 km) region in the northwestern Bering Sea (**Figs. 1a** and **1e**). Strong positive anomalies in chlorophyll-*a* during May also occurred in the southeastern Chukchi Sea (off the coast of Point Hope, Alaska), where values averaged ~16 mg m^{-3} higher than the 2003-2016 mean across a ~100 x 150 km area (**Figs. 1a** and **1e**). One additional positive anomaly of note occurred in the northern Barents Sea (west of Novaya Zemlya) during June (**Fig. 1f**), where 2017 values were ~8 mg m^{-3} higher than the 2003-2016 mean. These positive anomalies are in contrast to widespread negative chlorophyll anomalies across the Barents Sea in May (**Fig. 1e**). Other widespread negative anomalies occurred across Baffin Bay during May (**Fig. 1e**) and the Kara and Laptev seas during all months (**Figs. 1e**, **1f**, **1g** and **1h**).

Fig. 1. Mean monthly chlorophyll-*a* concentrations during 2017 are shown for (a) May, (b) June, (c) July and (d) August. (e-h) Monthly anomalies of chlorophyll-*a* concentrations for 2017 (relative to a 2003-2016 mean base period). Black areas (a-h) denote a lack of data owing to either clouds or sea ice. (i-l) Sea ice extent (designated by a 15% sea ice concentration threshold) based on passive microwave satellite data (Cavalieri et al., 1996; Maslanik and Stroeve, 1999) for the 2003-2016 mean (cyan line) and 2017 (magenta line). The locations A, B and C in (i) indicate the locations for the time series shown in **Fig. 3**. Satellite-based chlorophyll-*a* data across the pan-Arctic region were derived using the MODIS-Aqua Reprocessing 2014.0, OC3 algorithm: http://oceancolor.gsfc.nasa.gov/.

The most significant rates of change in the 2003-2017 satellite record in May have occurred southwest of Greenland in the Labrador Sea and to the west of Novaya Zemlya in the Barents Sea (**Fig. 2a**) and reflect increasing chlorophyll-*a* concentrations. The increase in the Barents Sea has been associated with declines in sea ice (**Fig. 1i**) linked to the Atlantic Water inflow (e.g., Alexeev et al., 2013). Positive trends are less pronounced but become increasingly widespread here during June, July and August (**Fig. 2b**, **2c** and **2d**).

Fig. 2. Linear trends in satellite-based chlorophyll-*a* data across the pan-Arctic region, derived using the MODIS-Aqua Reprocessing 2014.0, OC3 algorithm: http://oceancolor.gsfc.nasa.gov/. Theil-Sen median trends (2003-2017) in chlorophyll-*a* concentrations for each of the four months are shown, highlighting only statistically significant trends ($p < 0.1$, using the Mann-Kendall test for trend). Black areas indicate where data were insufficient to calculate trends (owing to the presence of sea ice and/or cloud coverage) and white areas indicate no trend.

To illustrate the quantitative nature of these trends, three example "hotspot" regions (shown in **Fig. 1i**) with notably steep trends in chlorophyll-*a* for May, June, July and August 2003-2017 are shown in **Fig. 3**. Statistically significant trends ($p < 0.1$) occur in the region in the Laptev Sea (A), northwest of the New Siberian Islands, during June (**Fig. 3a**); during all months (May, June, July and August) in the region in the Barents Sea (B), west of Novaya Zemlya (**Fig. 3b**); and during May in the region in the Labrador Sea (C), southwest of Greenland (**Fig. 3c**). The largest blooms take place in May for the Barents and Labrador sea sites, but are delayed until August for the Laptev Sea site owing to the later breakup of sea ice across that region. The largest increases in chlorophyll-*a* concentrations have occurred during May in the Labrador Sea (**Fig. 3c**) and the Barents Sea (**Fig. 3b**). In May 2017, there were relatively low chlorophyll-*a* concentrations at the Barents Sea site followed by relatively high concentrations in June (**Fig. 3b**). While many of these patterns are directly

linked to sea ice variability (and therefore light availability), it is important to note that there are other dominant factors at play that add to the complexity of observed chlorophyll-a concentrations, such as the distribution and availability of nutrients.

Fig. 3. Mean (±1 standard deviation) monthly chlorophyll-a concentrations (based on MODIS-Aqua satellite data) for May, June, July and August 2003-2017 for three example "hotspot" locations with notably steep trends in chlorophyll-a. Trends are shown for statistically significant ($p < 0.05$) time series only. The locations (shown in **Fig. 1i**) include (a) a ~22,500 km^2 region in the Laptev Sea northwest of the New Siberian Islands; (b) a ~25,400 km^2 region in the Barents Sea west of Novaya Zemlya; and (c) a 32,600 km^2 region in the Labrador Sea southwest of Greenland.

Primary Production

Chlorophyll-a concentrations give an estimate of the standing stock of algal biomass. Rates of primary production (i.e., the production of carbon via photosynthesis) give a slightly different perspective, and are calculated by combining chlorophyll-a concentrations with sea surface temperatures, incident solar irradiance, and mixed layer depths. Estimates of ocean primary productivity for nine regions (and the average of these nine regions) across the Arctic, relative to the 2003-2016 base period, indicate above average primary productivity for 2017 in all regions (**Fig. 4**, **Table 1**). Areas with the highest anomalies for 2017 include the Hudson Bay and Amerasian Arctic regions. In the longer term, positive trends in primary productivity occurred in all regions during the period 2003-2017 (**Fig. 4**, **Table 1**). Statistically significant trends occurred in the Eurasian Arctic, Barents Sea, Greenland Sea, Hudson Bay and North Atlantic, with the steepest trends found for the Barents Sea (15.9 g C/m^2/yr/dec) and the Eurasian Arctic (14.4 g C/m^2/yr/dec).

Fig. 4. Primary productivity (2003-2017, March-September only) in nine different regions of the Northern Hemisphere (for a definition of the regions see Comiso (2015)), as well as the average of these nine regions, derived using chlorophyll-*a* concentrations from MODIS-Aqua data, AVHRR sea surface temperature data, and additional parameters. Values are calculated based on the techniques described by Behrensfield and Falkowski (1997) and represent net primary productivity (NPP). Additional information regarding these data can be found in **Table 1**.

Table 1. Linear trends, statistical significance, percent change and primary productivity anomalies in 2017 (March-September) in the nine regions, and overall average, as shown in **Fig. 4**. Utilizing the Mann-Kendall test for trend, values in **bold** are significant at the 95% confidence level. The percent change is estimated from the linear regression of the 15-year time series.

Region	Trend, 2003-2017 (g C/m^2/yr/dec)	Mann-Kendall p-value	% Change	2017 Anomaly (g C/m^2/yr) from a 2003-2016 base period	2017 Anomaly (%) from a 2003-2016 base period
Eurasian Arctic	**14.38**	0.011	35.2	4.14	6.2
Amerasian Arctic	1.47	0.626	5.8	8.37	23.3
Sea of Okhotsk	4.06	0.282	8.1	2.14	2.9
Bering Sea	2.68	0.435	6.2	3.91	6.3
Barents Sea	**15.86**	0.000	30.7	1.65	2.0
Greenland Sea	**7.85**	0.003	19.2	0.02	0.0

Hudson Bay	**7.39**	0.011	26.7	12.39	28.8
Baffin Bay/Labrador Sea	6.32	0.093	16.8	6.13	10.8
North Atlantic	**7.97**	0.000	24.3	5.51	10.8
Average of Nine Regions	**7.55**	0.000	19.4	4.92	8.3

While similar trends have been reported previously for these regions using both SeaWiFS and MODIS data (Comiso, 2015), satellite evidence does suggest that recent increases in cloudiness have dampened the increases in production that would have otherwise occurred as a function of sea ice decline alone (Bélanger et al., 2013). Further challenges remain with linking primary productivity, as well depth-integrated chlorophyll biomass throughout the water column, to satellite-based surface chlorophyll-*a* values (Babin et al., 2015; Lee et al., 2015; Tremblay et al., 2015; Kahru, 2017). Satellite-based chlorophyll-*a* and primary productivity estimates continue to be confounded by issues such as river turbidity in coastal regions (e.g., Demidov et al., 2014; Chaves et al., 2015) and the presence of sea ice. Efforts to improve satellite retrieval algorithms based on in situ observations are thus critical to continue in all regions of the Arctic.

References

Alexeev, V. A., V. V. Ivanov, R. Kwok, and L. H. Smedsrud, 2013: North Atlantic warming and declining volume of arctic sea ice. *The Cryosphere Discuss.*, 7, 245-265, doi: 10.5194/tcd-7-245-2013.

Ardyna, M., M. Babin, E. Devred, A. Forest, M. Gosselin, P. Raimbault, and J. -É. Tremblay, 2017: Shelf-basin gradients shape ecological phytoplankton niches and community composition in the coastal Arctic Ocean (Beaufort Sea). *Limnology and Oceanography*, 62, 2113-2132, doi: 10.1002/lno.10554.

Babin, M., S. Bélanger, I. Ellinsten, A. Forest, V. Le Fouest, T. Lacour, M. Ardyna, and D. Slagstad, 2015: Estimation of primary production in the Arctic Ocean using ocean colour remote sensing and coupled physical-biological models: Strengths, limitations and how they compare. *Progress in Oceanography*, 139, 197-220, doi: 10.1016/j.pocean.2015.08.008.

Barber, D. G., H. Hop, C. J. Mundy, B. Else, I. A. Dmitrenko, J. -É. Tremblay, J. K. Ehn, P. Assmy, M. Daase, L. M. Candlish, and S. Rysgaard, 2015: Selected physical, biological and biogeochemical implications of a rapidly changing Arctic Marginal Ice Zone. *Progress in Oceanography*, 139, 122-150, doi: 10.1016/j.pocean.2015.09.003.

Behrenfeld, M. J., and P. G. Falkowski, 1997: Photosynthetic rates derived from satellite-based chlorophyll concentration. *Limnology and Oceanography*, 42(1), 1-20.

Bélanger, S., M. Babin, and J. -É. Tremblay, 2013: Increasing cloudiness in Arctic damps the increase in phytoplankton primary production due to sea ice receding. *Biogeosciences*, 10, 4087-4101, doi: 10.5194/bg-10-4087-2013.

Cavalieri, D. J., C. L. Parkinson, P. Gloersen, and H. Zwally, 1996, updated yearly: Sea Ice Concentrations from Nimbus-7 SMMR and DMSP SSM/I-SSMIS Passive Microwave Data. [2003-2014]. Boulder, Colorado, USA: NASA DAAC at the National Snow and Ice Data Center.

Chaves, J., P. J. Werdell, C. W. Proctor, A. R. Neeley, S. A. Freeman, C. S. Thomas, and S. B. Hooker, 2015: Assessment of ocean color data records from MODIS-Aqua in the western Arctic Ocean. *Deep-Sea Research II-Part A*, 118, 32-43, doi: 10.1016/j.dsr2.2015.02.011.

Comiso, J. C., 2015: Variability and trends of the global sea ice covers and sea levels: Effects on physicochemical parameters in *Climate and Fresh Water Toxins*, L. M. Botana, M. C. Lauzao, and N. Vilarino, Eds., De Gruyter, Berlin, Germany.

Demidov, A. B., S. A. Mosharov, and P. N. Makkaveev, 2014: Patterns of the Kara Sea primary production in autumn: Biotic and abiotic forcing of subsurface layer. *Journal of Marine Systems*, 132, 130-149, doi: 10.1016/j.jmarsys.2014.01.014.

Hill, V., M. Ardyna, S. H. Lee, and D. E. Varela, 2017: Decadal trends in phytoplankton production in the Pacific Arctic Region from 1950 to 2012. *Deep-Sea Research Part II*, http://dx.doi.org/10.1016/j.dsr.2016.12.015.

Kahru, M., 2017: Ocean productivity from space: Commentary. *Global Biogeochem. Cycles*, 31, 214-216, doi: 10.1002/2016GB005582.

Lee, Y. J., et al., 2015: An assessment of phytoplankton primary productivity in the Arctic Ocean from satellite ocean color/in situ chlorophyll-*a* based models. *Journal of Geophysical Research-Oceans*, 120, 6508-6541, doi: 10.1002/2015JC011018.

Leu, E., C. J. Mundy, P. Assmy, K. Campbell, T. M. Gabrielsen, M. Gosselin, T. Juul-Pedersen, and R. Gradinger, 2015: Arctic spring awakening - Steering principles behind the phenology of vernal ice algal blooms. *Progress in Oceanography*, 139, 151-170, http://dx.doi.org/10.1016/j.pocean.2015.07.012.

Maslanik, J., and J. Stroeve, 1999, updated daily: Near-Real-Time DMSP SSM/I-SSMIS Daily Polar Gridded Sea Ice Concentrations. [2016]. Boulder, Colorado, USA: NASA DAAC at the National Snow and Ice Data Center.

Müller-Karger, F. E., R. Varela, R. Thunell, R. Luerssen, C. Hu, and J. J. Walsh, 2005: The importance of continental margins in the global carbon cycle. *Geophysical Research Letters*, 32, L01602, doi: 10.1029/2004GL021346.

Tremblay, J. -É., L. G. Anderson, P. Matrai, S. Bélanger, C. Michel, P. Coupel, and M. Reigstad, 2015: Global and regional drivers of nutrient supply, primary production and CO_2 drawdown in the changing Arctic Ocean. *Progress in Oceanography*, 139, 171-196, doi: 10.1016/j.pocean.2015.08.009.

November 30, 2017

Tundra Greenness

H. Epstein[1], U. Bhatt[2], M. Raynolds[3], D. Walker[3], B. C. Forbes[4], T. Horstkotte[5], M. Macias-Fauria[6], A. Martin[7], G. Phoenix[8], J. Bjerke[9], H. Tømmervik[9], P. Fauchald[9], H. Vickers[10], R. Myneni[11], C. Dickerson[1]

[1]Department of Environmental Sciences, University of Virginia, Charlottesville, VA, USA

[2]Geophysical Institute, University of Alaska Fairbanks, Fairbanks, AK, USA

[3]Institute of Arctic Biology, University of Alaska Fairbanks, Fairbanks, AK, USA

[4]Arctic Centre, University of Lapland, Rovaniemi, Finland

[5]Department of Ecology and Environmental Sciences, Umeå University, Umeå, Sweden

[6]School of Geography and the Environment, Oxford University, Oxford, UK

[7]Department of Zoology, Oxford University, Oxford, UK

[8]Department of Animal and Plant Sciences, University of Sheffield, Sheffield, UK

[9]Norwegian Institute for Nature Research, Tromsø, Norway

[10]Norut Northern Research Institute, Tromsø, Norway

[11]Department of Earth and Environment, Boston University, Boston, MA, USA

Highlights

- Tundra greenness has increased substantially throughout the Arctic over the past two years (2015-2016), following 3-4 years of continuous declines.
- Peak tundra greenness for 2016 ranks 4th (entire Arctic), 9th (Eurasian Arctic), and 3rd (North American Arctic) in the context of the 35-year record.
- Long-term trends (1982-2016) show greening on the North Slope of Alaska, the southern Canadian tundra, and in the central Siberian tundra; tundra browning is found in western Alaska (Yukon-Kuskokwim Delta), the higher-Arctic Canadian Archipelago, and western Siberian tundra.

Vegetation in the Arctic tundra has been responding to environmental changes over the course of the last several decades, with the tendency being an increase in the quantity of above-ground vegetation (i.e., "greening"). These vegetation changes vary spatially throughout the circumpolar Arctic in both direction and magnitude, and they are not always consistent over time. This suggests complex interactions among atmosphere, ground (soils and permafrost), vegetation, and herbivore components of the Arctic system. Changes in tundra vegetation can have important effects on permafrost, hydrological dynamics, carbon and nutrient cycling, and the surface energy balance (e.g., Frost et al., 2017; Kępski et al., 2017), as well as the diversity, abundance, and distribution of both wild and domesticated herbivores in the Arctic (e.g., Fauchald et al., 2017; Horstkotte et al., 2017). We continue to evaluate the state of the circumpolar Arctic vegetation, to improve our understanding of these complex interactions and their impacts on the Arctic system and beyond.

Using Earth-Observing Satellites (EOS) with daily return intervals, Arctic tundra vegetation has been continuously monitored since 1982. We report on data from the Global Inventory Modeling and Mapping Studies (GIMMS) version 3g dataset (GIMMS, 2013) based largely on the Advanced Very High Resolution Radiometer (AVHRR) sensors onboard NOAA satellites (Pinzon and Tucker, 2014). At the time of the writing of this report, the GIMMS3g dataset was only available through 2016. The GIMMS product (at ~12-km resolution for this report) is a bi-weekly, maximum-value composited dataset of the Normalized Difference Vegetation Index (NDVI). NDVI is highly correlated with aboveground vegetation (e.g., Raynolds et al., 2012), or "greenness," within the Arctic tundra. We use two metrics based on the NDVI: MaxNDVI and TI-NDVI. Max NDVI is the peak NDVI for the year (growing season), and is related to yearly maximum aboveground vegetation biomass. TI (time-integrated) NDVI is the sum of the bi-weekly NDVI values for the growing season, and is correlated with the total aboveground vegetation productivity.

Examining the overall trend in tundra greenness for the now 35-year record (1982-2016), it is apparent that the MaxNDVI has increased throughout a majority of the geographic circumpolar Arctic tundra (**Fig. 1 a**). Widespread increase is also true, though to a lesser extent, for TI-NDVI (**Fig. 1b**). Regions with some of the greatest increases in tundra greenness are the North Slope of Alaska, the Low Arctic (southern tundra subzones) of the Canadian tundra, and east of the Taimyr Peninsula in north-central Siberia, Russia. However, tundra greenness has declined (i.e., "browning") on the Yukon-Kuskokwim Delta of western Alaska, the High Arctic of the Canadian Archipelago, and the north-western Siberian tundra. Whereas the regions of browning (NDVI decrease) tend to be collocated between MaxNDVI and TI-NDVI, the decrease in TI-NDVI covers a greater areal extent than that of MaxNDVI. A particular region of note includes the Yamal, Gydan, and Taimyr peninsulas in north-western Siberia, which generally show increases in MaxNDVI, yet decreases in TI-NDVI over the course of the record.

Fig. 1a. Magnitude of the trend in maximum (Max)NDVI from 1982-2016.

Fig. 1b. Magnitude of the trend in temporal-integrated (TI)-NDVI from 1982-2016.

Following 3-4 years of successive declines prior to and including 2014, the NDVI for Arctic tundra exhibited an upturn in 2015 (**Fig. 2**). The one exception was the TI-NDVI for North America, which continued to decrease in 2015. The NDVI then increased from 2015 to 2016 for both indices and both continents, with the past two years exhibiting substantial recovery from the prior years of "browning." MaxNDVI and TI-NDVI for the entire Arctic increased 3.2% and 5.3%, respectively, between 2015 and 2016. Much of this can be attributed to enhanced NDVI in North America with increases of 6.5% and 9.2%, respectively, for MaxNDVI and TI-NDVI. This is the first annual increase in TI-NDVI for North America since 2010.

Fig. 2a. Maximum (Max)NDVI from 1982 to 2016 for North America (bottom), Eurasia (top), and the Arctic as a whole (middle).

Fig. 2b. Time-integrated (TI)-NDVI from 1982 to 2016 for North America (bottom), Eurasia (top), and the Arctic as a whole (middle).

All NDVI values for 2016 were greater than their respective mean values for the 35-year record, with the exception of TI-NDVI for Eurasia. MaxNDVI values ranked 4th, 9th, and 3rd greatest for the Arctic, Eurasian Arctic, and North American Arctic, respectively. TI-NDVI values ranked 14th, 24th, and 2nd for the Arctic, Eurasian Arctic, and North American Arctic, respectively, indicating a large discrepancy in the dynamics of TI-NDVI between the Eurasian and North American continents. Based on remotely-sensed Land Surface Temperatures (LST), from the same sensors as those providing the NDVI values, the Summer Warmth Index (SWI - sum of mean monthly temperatures > 0° C) for the Arctic as a whole and for the Eurasian Arctic was greater in 2016 than in any other year of the satellite record (since 1982). For the North American Arctic, the 2016 SWI was the 2nd greatest on record.

The reported controls on tundra greening are numerous and varied, and include increases in summer, spring, and winter temperatures, as well as growing season length (Bhatt et al., 2017; Fauchald et al., 2017; Horstkotte et al., 2017; Myers-Smith and Hik, 2017; Vickers et al., 2017), in part controlled by reductions in Arctic Ocean sea-ice

cover (Bhatt et al., 2017; Macias-Fauria et al., 2017). Other controls on tundra greening include increases in snow water equivalent and soil moisture, increases in active layer depth, changes in the patterns of herbivore activity, and even a reduction in the human use of the land (Fauchald et al., 2017; Horstkotte et al., 2017; Martin et al., 2017; Westergaard-Nielsen et al., 2017).

Even though the past two years have seen large increases in tundra NDVI, there are still regions of the Arctic that have experienced "browning" (i.e., decreases in tundra NDVI) over the length of the satellite record, and there have been substantive time periods of tundra browning, even within a general greening trend. While research on tundra browning is still relatively sparse, there has recently been greater attention given to this phenomenon. Bjerke et al. (2017) report on extensive vegetation dieback in northern Norway (including Svalbard) in 2014 and 2015, and attributed this largely to changes in winter climate–specifically, reductions in snow cover due to winter warming events leave the ground exposed to subsequent freezing and desiccation (Vikhamar-Schuler et al., 2016); insect outbreaks contributed secondarily to vegetation mortality.

References

Bhatt, U., D. Walker, R. Raynolds, P. Bieniek, H. Epstein, J. Comiso, C. Tucker, M. Steele, W. Ermold, and J. Zhang, 2017: Changing seasonality of Panarctic tundra vegetation in relationship to climatic variables. *Environ. Res. Lett.*, 12, 055003.

Bjerke, J. W., R. Treharne, D. Vikhamar-Schuler, S. R. Karlsen, V. Ravolainen, S. Bokhorst, G. K. Phoenix, Z. Bochenek, and H. Tømmervik, 2017: Understanding the drivers of extensive plant damage in boreal and Arctic ecosystems: Insights from field surveys in the aftermath of damage. *Sci. Tot. Environ.*, doi: 10.1016/j.scitotenv.2017.05.050.

Fauchald, P., T. Park, H. Tømmervik, R. Myneni, and V. Helene Hauser, 2017: Arctic greening from warming promotes declines in caribou populations. *Sci. Adv.*, 3, e1601365.

Frost, G. V., H. E. Epstein, D. A. Walker, G. Matyshak, and K. Ermokhina, 2017: Seasonal and long-term changes in active-layer temperatures after tall shrubland expansion and succession in Arctic tundra. *Ecosystems*, 16, 1296.

Global Inventory Modeling and Mapping Studies (GIMMS), 2013: Available online: http://gcmd.nasa.gov/records/GCMD_GLCF_GIMMS.html.

Horstkotte, T., T. Utsi, Å. Larsson-Blind, P. Burgess, B. Johansen, J. Käyhkö, L. Oksanen, and B. C. Forbes, 2017: Human-animal agency in reindeer management: herders' perspectives on vegetation dynamics under climate change. *Ecosphere*, 8(9), e01931, doi: 10.1002/ecs2.1931.

Kępski, D., B. Luks, K. Migala, T. Wawrzyniak, S. Westermann, and B. Wojtuń, 2017: Terrestrial remote sensing of snowmelt in a diverse High-Arctic tundra environment using time-lapse imagery. *Remote Sens.*, 9, 733.

Macias-Fauria, M., S. R. Karlsen, and B. C. Forbes, 2017: Disentangling the coupling between sea ice and tundra productivity in Svalbard. *Sci. Reports*, 7, 8586.

Martin, A. C., E. S. Jeffers, G. Petrokofsky, I. Myers-Smith, and M. Macias-Fauria, 2017: Shrub growth and expansion in the Arctic tundra: an assessment of controlling factors using an evidence-based approach. *Environ. Res. Lett.*, 12, 085007.

Myers-Smith, I. H., and D. S. Hik, 2017: Climate warming as a driver of tundra shrubline advance. *J. Ecol.*, doi: 10.1111/1365-2745.12817.

Pinzon, J., and C. Tucker, 2014: A non-stationary 1981-2014 AVHRR NDVI3g time series. *Remote Sens.*, 6, 6929-6960, doi: 10.3390/rs6086929.

Raynolds, M. K., D. A. Walker, H. E. Epstein, J. E. Pinzon, and C. J. Tucker, 2012: A new estimate of tundra-biome phytomass from trans-Arctic field data and AVHRR NDVI. *Remote Sens. Lett.*, 3, 403-411.

Vickers, H., K. A. Høgda, S. Solbø, S. R. Karlsen, H. Tømmervik, R. Aanes, and B. Hansen, 2016: Change in greening in the high Arctic: insights from a 30 year AVHRR max NDVI dataset for Svalbard. *Environ. Res. Lett.*, 11, 105004.

Vikhamar-Schuler, D., K. Isaksen, J. E. Haugen, H. Tømmervik, B. Luks, T. Vikhamar Schuler, and J. W. Bjerke, 2016: Change in winter warming events in the Nordic Arctic Region. *J. Clim.*, doi: 10.1175/JCLI-D-15-0763.1.

Westergaard-Nielsen, A., M. Lund, S. H. Pedersen, N. M. Schmidt, S. Klosterman, J. Abermann, and B. U. Hansen, 2017: Transitions in high-Arctic vegetation growth patterns and ecosystem productivity tracked with automated cameras from 2000 to 2013. *Ambio*, 46, S39-S52.

November 17, 2017

Terrestrial Permafrost

V. E. Romanovsky[1], S. L. Smith[2], K. Isaksen[3], N. I. Shiklomanov[4], D. A. Streletskiy[4], A. L. Kholodov[1], H. H. Christiansen[5], D. S. Drozdov[6,7], G. V. Malkova[6], S. S. Marchenko[1]

[1]Geophysical Institute, University of Alaska Fairbanks, Fairbanks, AK, USA

[2]Geological Survey of Canada, Natural Resources Canada, Ottawa, ON, Canada

[3]Norwegian Meteorological Institute, Oslo, Norway

[4]Department of Geography, George Washington University, Washington, DC, USA

[5]Geology Department, University Centre in Svalbard, UNIS, Norway

[6]Earth Cryosphere Institute, Tyumen Science Center, Tyumen, Russia

[7]Tyumen State University, Tyumen, Russia

Highlights

- In 2016, permafrost temperatures were the highest on record at the majority of Arctic observation sites.
- Increases in permafrost temperature since 2000 have been greatest in cold permafrost of the Alaskan Arctic, Canadian high Arctic, and Svalbard.
- The rates of increase in ground temperatures at colder permafrost sites coincide with the rate of increase in the Arctic surface air temperatures.

Permafrost is an important component of the Arctic landscape, influencing hydrological systems and ecosystems and also presenting challenges to infrastructure development. Permafrost temperature and active layer thickness are key indicators of changes in permafrost conditions. Permafrost is defined as earth materials that exist at or below 0° C continuously for at least two consecutive years. The active layer is the seasonally thawed layer above the permafrost. Permafrost temperatures, at a depth where seasonal temperature variations are negligible, can provide a good indication of long-term change. On the other hand, the active layer responds to shorter term fluctuations in climate and is especially sensitive to changes in summer air temperature and precipitation. Warming (increasing permafrost temperatures) and thawing (melting of the ice in frozen ground) of permafrost in the Arctic are reported in this essay.

Changes up to 2016 (most recent data available) in mean annual permafrost temperatures and ALT (active layer thickness) are summarized for a number of sites throughout the Arctic (**Fig. 1**) (http://gtnpdatabase.org/, http://permafrost.gi.alaska.edu/sites_map, https://www2.gwu.edu/~calm/data/data-links.html). Recent long-term changes in permafrost temperature are driven mostly by the surface air temperature trends (Romanovsky et al., 2015). Other important factors for permafrost temperature, such as snow cover, vegetation and soil moisture, do not yet show pronounced regional long-term trends. 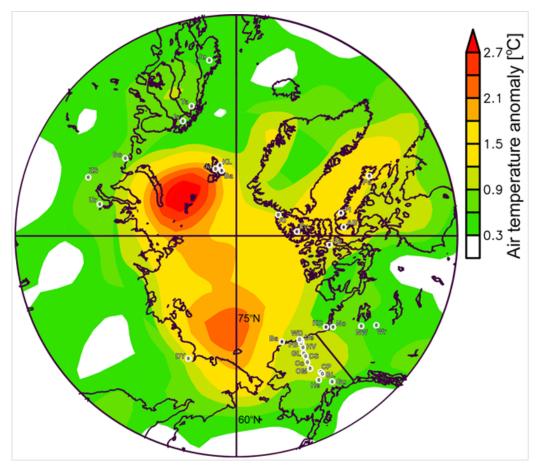In general, the increase in permafrost temperatures observed since the 1980s is more substantial in the higher latitudes where the largest increase in surface air temperature is also observed.

Fig. 1. Location of the permafrost monitoring sites shown in **Fig. 2** superimposed on average surface air temperature anomalies during 2000-2016 (with respect to the 1981-2010 mean) from the NCEP-reanalysis (Kalnay et al. 1996). Data provided by the NOAA/ESRL Physical Sciences Division, Boulder, CO (www.esrl.noaa.gov/psd/). Sites shown in **Fig.2** are: a) Barrow (Ba), West Dock (WD), KC-07 (KC), Duvany Yar (DY), Deadhorse (De), Franklin Bluffs (FB), Galbraith Lake (GL), Happy Valley (HV), Norris Ck (No); b) College Peat (CP), Old Man (OM), Chandalar Shelf (CS), Birch Lake (BL), Coldfoot (Co), Norman Wells (NW), Wrigley 2 (Wr), Healy (He), Gulakana (Gu), Wrigley 1 (Wr); c) Eureka EUK4 (Eu), Alert BH2 (Al), Alert BH5 (Al), Resolute (Re), Alert BH1 (Al), Arctic Bay (AB), Pond Inlet (PI), Pangnirtung (Pa); d) Janssonhaugen (Ja), Bayelva (Ba), Kapp Linne 1 (KL), Urengoy #15-10 (Ur), Juvvasshøe (Ju), Tarfalaryggen (Ta), Polar Ural (ZS), Bolvansky #59 (Bo), Bolvansky #65 (Bo), Urengoy #15-06 (Ur), Bolvansky #56 (Bo), Iskoras Is-B-2 (Is).

Permafrost Temperatures

In 2016, record high temperatures at 20-m depth occurred at all permafrost observatories on the North Slope of Alaska except Deadhorse (**Fig 2a**) (Romanovsky et al., 2017). Since 2000, temperature at 20-m depth in this region has increased between 0.21° C and 0.66° C per decade (**Fig. 2a**; **Table 1**). Following the slight cooling of 2007-2013, permafrost temperatures increased in Interior Alaska at all sites, with especially strong increase at Birch Lake, associated with a new record high in 2016 for the entire 32 years of measurements (**Fig. 2b**; **Table 1**).

In northwestern Canada, the temperature of permafrost in the central Mackenzie Valley has generally increased since the mid-1980s, with less warming observed since 2000 (Norman Wells and Wrigley in **Fig. 2b**; **Table 1**), corresponding to a period of steady air temperatures (Smith et al., 2016). In contrast, greater recent warming has been observed in the colder permafrost of the northern Mackenzie (Norris Ck, KC-07 in **Fig. 2a; Table 1**), reflecting relatively higher increase in air temperatures over the last decade in this region (**Fig. 1**) (Smith et al., 2016).
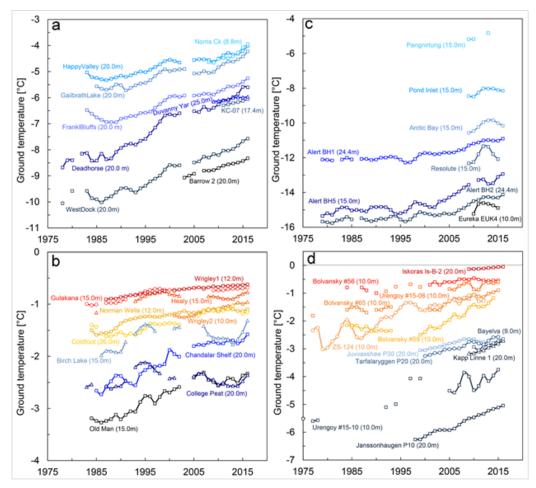
Fig. 2. Time series of mean annual ground temperature at depths of 9 to 26 m below the surface at selected measurement sites that fall roughly into the Adaptation Actions for a Changing Arctic Project (https://www.amap.no/adaptation-actions-for-a-changing-arctic-part-c) priority regions: a) cold continuous permafrost of NW North America and NE of East Siberia (Beaufort-Chukchi region); b) discontinuous permafrost in Alaska and northwestern Canada; c) cold continuous permafrost of Eastern and High Arctic Canada (Baffin Davis Strait); d) continuous to discontinuous permafrost in Scandinavia, Svalbard, Russia/Siberia (Barents region). Temperatures are measured at or near the depth of zero annual amplitude. Data series are updated from Christiansen et al. (2010), Romanovsky et al. (2015), Smith et al. (2015, 2016), Ednie and Smith (2015), Boike et al. (2017).

In northeastern Canada, the most recent mean permafrost temperatures in the upper 25 m of the ground at Alert, northernmost Ellesmere Island in the high Arctic, were among the highest recorded since 1978 (**Fig. 2c**). Although permafrost at Alert has generally warmed since 1978, the highest rate of permafrost temperature increase occurred between 2000-2010 (**Table 1**) (Smith et al., 2015), consistent with air temperature trends (**Fig. 1**). There has been little change since 2010 (**Fig. 2c**), which coincides with a period of lower surface air temperatures. Short records, from other sites to the south in the Queen Elizabeth Islands (Resolute and Eureka) and on Baffin Island (Pond Inlet, Arctic Bay) show a general warming of permafrost at 10-15 m depth since 2008 (**Fig. 2c**, **Table 1**) with some cooling since 2012. The difference between the regional tendencies in permafrost temperature is likely related to regional variation is surface air temperatures. Since 2012, there was a greater decrease in air temperature at Eureka and other sites farther south compared to Alert. Also, at the relatively shallow measurement depths, there remains some influence from seasonal variation in the ground temperatures. Therefore, ground temperature at the shallower sites are more responsive to shorter term fluctuations in air temperature.

Increases in permafrost temperature over the last 30-35 years in northern Russia have been similar to those in northern Alaska and the Canadian high Arctic. In the Russian European North and western Siberian Arctic, temperatures at 10-m depth have increased by ~0.4° C to 0.6° C decade[-1] since the late 1980s at colder permafrost sites (**Fig. 2d**, Bolvansky #59, Urengoy #15-6 and #15-10) with less warming

in warmer permafrost (**Table 1**, **Fig. 2d**, sites Bolvansky #56 and Urengoy #15-6; Drozdov et al., 2015). In these regions the differences in permafrost temperature (cold vs. warm) exist because of differences in surface conditions related to different types of landscape, while climatic conditions are largely consistent.

In Nordic regions, warming and thawing of permafrost have been observed recently (Christiansen et al., 2010; Isaksen et al., 2011; Farbrot et al., 2013). Since 2000, temperature at 20-m depth has increased between 0.1° C and 0.7° C per decade (**Fig. 2d**, **Table 1**). Lower rates of increase occur where permafrost temperatures are close to 0° C and latent heat effects related to melting ground ice in fine-grained material are important. Greater warming occurred in colder permafrost on Svalbard and in northern Scandinavia (**Table 1**). In the discontinuous permafrost zone of southern Norway, permafrost warmed in 2015 and 2016, following a period of cooling between 2011 and 2014 (**Fig. 2d**).

Active Layer Thickness

The average active-layer thickness (ALT; determined by mechanical probing and typically accurate to 0.5 cm) in 2016 for 20 North Slope sites was 0.52 m, which is 4 cm greater than the 1996-2016 average (**Fig. 3**). This value represents the 21-year maximum, which was previously achieved in 1998 and 2013 (**Fig. 3**). In the interior of Alaska ALT has on average increased by 0.14 m in 2016 compared to 2015 values. Three out of four Alaska Interior sites with 20 years of continuous observations reported absolute maximum ALT values in 2016. The previous maxima at these sites was achieved in 2015.

Fig. 3. Long-term active-layer change in six different Arctic regions as observed by the Circumpolar Active Layer Monitoring (CALM) program. The data are presented as annual anomalies (in m) from the mean value for the period of observations indicated for each region. Thaw depth observations from the end of the thawing season were used. Only sites with at least 15 years of continuous thaw depth observations are shown in the figure.

Records from 25 sites with thaw tubes in the Mackenzie Valley, northwestern Canada, indicate that overall there has been a general increase in ALT in this region since 2008 with a peak value occurring in 2012, about 10% greater than the 2003-2012 mean (Duchesne et al., 2015; Smith et al., 2016). Although ALTs were lower after 2012, they are on average greater than the 2003-2012 mean.

In West Siberia, the active-layer thickness increased by an average of 0.16 m in 2016, reaching 1.45 m, the highest recorded thickness in 20 years of observations. The previous maximum was 1.29 m in 2015. Similarly, the ALT in 2016 has substantially increased in Russian European North. Slight ALT increase in 2016 was observed in East Siberia and Chukotka (Russian Far East) (**Fig. 3**). In central Siberia ALT remained unchanged in 2016.

Significant (0.15 m) ALT increase in 2016 was reported for Greenland sites. Such increase has reversed a monotonic ALT decline observed since 2010. Similarly, the increase in ALT was observed on Svalbard where 2016 active-layer thickness reached its maximum and increased by 15% compared to the 2000-2015 mean.

In the Nordic countries, active layer records (1999-2016) indicate a general increase of 0.10 to 0.30 m in ALT since 1999. The summer of 2014 was particularly warm in the Nordic countries and contributed to the thickest active layer measured so far at some places.

Table 1. Change in mean annual ground temperature (MAGT; °C per decade) for sites shown in **Fig. 2**, for which data are available for 2016. For sites with records initiated prior to 2000, the rate for the entire available record is provided as well as the rate for the period after 2000. The names of the stations with record high temperatures in 2016 are shown in red. (Note records for some sites only began after 2007 as shown in **Fig. 2**).

Region	Sites	Entire Record (see **Fig. 2**)	Since 2000
Alaskan Arctic plain	West Dock (**WD**), Deadhorse (**De**), Franklin Bluffs (**FB**), Barrow (**Ba**)	+0.36 to +0.8	+0.44 to +0.65
Northern foothills of the Brooks Range, Alaska	Happy Valley (**HV**), Galbraith Lake (**GL**)	+0.3 to +0.42	+0.34 to +0.47
Southern foothills of the Brooks Range, Alaska	Coldfoot (**Co**), Chandalar Shelf (**CS**), Old Man (**OM**)	+0.08 to +0.35	+0.14 to +0.25
Interior Alaska	College Peat (**CP**), Birch Lake (**BL**), Gulkana (**Gu**), Healy (**He**)	+0.07 to +0.22	+0.03 to +0.1
Central Mackenzie Valley	Norman Wells (**NW**), Wrigley (**Wr**)	Up to +0.1	<+0.1 to +0.2
Northern Mackenzie Valley	Norris Ck (**No**), KC-07 (**KC**)	NA	+0.4 to +0.8
Baffin Island	Pond Inlet (**PI**), Arctic Bay	NA	+0.5 to +0.7
High Canadian Arctic	Resolute (**Re**), Eureka (**Eu**)	NA	+0.4 to +0.7
High Canadian Arctic	Alert (**Al**) @ 15 m 24 m	+0.5 +0.3 to +0.4	+1.2 +0.7 to +1
North of East Siberia	Duvany Yar (**DY**)		+0.3
North of West Siberia	Urengoy 15-06 and 15-10 (**Ur**)	+0.31 to +0.47	+0.1 to +0.19
Russian European North	Bolvansky 56, 59, and 65 (**Bo**), Polar Ural (ZS-124)	+0.18 to +0.46	+0.1 to +0.83
Svalbard	Janssonhaugen (**Ja**), Bayelva (**Ba**), Kapp Linne 1 (**KL**)	+0.7	+0.6 to +0.7
Northern Scandinavia	Tarfalarggen (**Ta**), Iskoras Is-B-2 (**Is**)	NA	+0.1 to +0.4
Southern Norway	Juvvasshøe (**Ju**)	+0.2	+0.2

References

Boike, J., I. Juszak, S. Lange, S. Chadburn, E. Burke, P. P. Overduin, K. Roth, O. Ippisch, N. Bornemann, L. Stern, I. Gouttevin, E. Hauber, and S. Westermann, 2017: A 20-year record (1998-2017) of permafrost, active layer, and meteorological conditions at a High Arctic permafrost research site (Bayelva, Spitsbergen): an opportunity to validate remote sensing data and land surface, snow, and permafrost models, *Earth System Science Data Discussions*, 1-86, doi: 10.5194/essd-2017-100.

Christiansen, H. H., B. Etzelmüller, K. Isaksen, H. Juliussen, H. Farbrot, O. Humlum, M. Johansson, T. Ingeman-Nielsen, L. Kristensen, J. Hjort, P. Holmlund, A. B. K. Sannel, C. Sigsgaard, H. J. Åkerman, N. Foged, L. H. Blikra, M. A. Pernosky, and R. Ødegård, 2010: The thermal state of permafrost in the Nordic area during the International Polar Year, *Permafrost and Periglacial Processes*, 21, 156-181, doi: 10.1002/ppp.687.

Drozdov, D., Y. Rumyantseva, G. Malkova, V. Romanovsky, A. Abramov, P. Konstantinov, D. Sergeev, N. Shiklomanov, A. Kholodov, O. Ponomareva, and D. Streletskiy, 2015: Monitoring of permafrost in Russia and the international GTN-P project. 68th Canadian Geotechnical Conference - GEOQuébec 2015, Québec, Canada, September 20-23, 2015.

Duchesne, C., S. L. Smith, M. Ednie, and P. P. Bonnaventure, 2015: Active layer variability and change in the Mackenzie Valley, Northwest Territories. Paper 117. In GEOQuébec 2015 (68th Canadian Geotechnical Conference and 7th Canadian Conference on Permafrost). Québec. GEOQuébec 2015 Organizing Committee.

Ednie, M., and S. L. Smith, 2015: Permafrost temperature data 2008-2014 from community based monitoring sites in Nunavut, Geological Survey of Canada Open File, 7784.

Farbrot, H., K. Isaksen, B. Etzelmüller, and K. Gisnås, 2013: Ground thermal regime and permafrost distribution under a changing climate in northern Norway. *Permafrost and Periglacial Processes*, 24, 20-38. doi: 10.1002/ppp.1763.

Isaksen, K., R. S. Ødegård, B. Etzelmüller, C. Hilbich, C. Hauck, H. Farbrot, T. Eiken, H. O. Hygen, and T. F. Hipp, 2011: Degrading mountain permafrost in southern Norway: spatial and temporal variability of mean ground temperatures, 1999-2009, *Permafrost and Periglacial Processes*, 22, 361-377, doi: 10.1002/ppp.728.

Kalnay, E., M. Kanamitsu, R. Kistler, W. Collins, D. Deaven, L. Gandin, M. Iredell, S. Saha, G. White, J. Woollen, Y. Zhu, A. Leetmaa, R. Reynolds, M. Chelliah, W. Ebisuzaki, W. Higgins, J. Janowiak, K. C. Mo, C. Ropelewski, J. Wang, R. Jenne, and D. Joseph, 1996: The NCEP/NCAR 40-Year Reanalysis Project. *Bulletin of American Meteorological Society*, 77, 437-471, doi: 10.1175/1520-0477(1996)077<0437: TNYRP>2.0.CO;2.

Romanovsky, V. E, W. L. Cable, and A. L. Kholodov, 2015: Changes in Permafrost and Active-layer Temperatures along an Alaskan Permafrost-Ecological Transect. Paper 479. In GEOQuébec 2015 (Proceedings 68th Canadian Geotechnical Conference and 7th Canadian Conference on Permafrost). Québec. GEOQuébec 2015 Organizing Committee.

Romanovsky, V. E., S. L. Smith, N. I. Shiklomanov, D. A. Streletskiy, K. Isaksen, A. L. Kholodov, H. H. Christiansen, D. S. Drozdov, G. V. Malkova, and S. S. Marchenko, 2017: [Arctic] Terrestrial Permafrost [in "State of the Climate in 2016"]. *Bulletin of the American Meteorological Society* (supplement), 98(8): S147-S151.

Smith, S. L., A. G. Lewkowicz, C. Duchesne, and M. Ednie, 2015: Variability and change in permafrost thermal state in northern Canada. Paper 237. In GEOQuébec 2015 (Proceedings 68th Canadian Geotechnical Conference and 7th Canadian Conference on Permafrost). Québec. GEOQuébec 2015 Organizing Committee.

Smith, S. L., J. Chartrand, C. Duchesne, and M. Ednie, 2016: Report on 2015 field activities and collection of ground thermal and active layer data in the Mackenzie Corridor, Northwest Territories, Geological Survey of Canada Open File 8125.

November 28, 2017

Groundfish Fisheries in the Eastern Bering Sea

S. Zador[1], K. Holsman[1], J. Ianelli[1], E. Siddon[2], A. Whitehouse[1]

[1]Resource Ecology and Fisheries Management Division, Alaska Fisheries Science Center, National Marine Fisheries Service,
National Oceanic and Atmospheric Administration, 7600 Sand Point Way NE, Seattle, WA 98115, USA

[2]Auke Bay Laboratories, Alaska Fisheries Science Center, National Marine Fisheries Service,
National Oceanic and Atmospheric Administration, 17109 Point Lena Loop Rd, Juneau, AK 99801, USA

Highlights

- The eastern Bering Sea supports one of the largest fisheries in the world: walleye pollock (*Gadus chalcogrammus*).
- The annual cycle of sea ice cover in the eastern Bering Sea influences ecosystem productivity via the formation of a cold pool of bottom water that varies in extent each year.
- Years with extensive cold pools are typified by energy-rich foodwebs, which favor walleye pollock and their preferred prey. However, multiple studies predict overall declines in the intensity and extent of cold pools under future warming conditions.
- Better scientific understanding of how ecosystem components interact enables ecosystem science to inform fisheries management practices that are robust to future warming.

The Eastern Bering Sea (EBS) is a highly productive ecosystem characterized by a broad (>500 km) continental shelf (defined as <200 m) and narrow slope to a deep-sea basin (**Fig. 1**, Stabeno et al., 1999). Commercial fisheries in the EBS represent over 40% of fish landed annually in US waters, and the system has long supported one of the largest fisheries in the world: walleye pollock (*Gadus chalcogrammus*; hereafter pollock; FAO, 2017; Fissel et al., 2016). In addition to pollock, key commercial fisheries include King, snow and Tanner crab, Pacific cod, yellowfin sole, Pacific halibut, other flatfish, salmon and Pacific herring. The US federal government is responsible for sustainably managing the groundfish species, which include the bottom or near-bottom dwelling pollock, Pacific cod, rockfish and a variety of flatfish. While there is currently no commercial fishing allowed in US Arctic waters north of the EBS, there is awareness that warming oceans may extend the distributions of some fish species northward, increasing the potential for commercial fishing and associated vessel traffic (Cheung et al., 2015; Pinsky et al., 2013; Haynie and Pfeiffer, 2013).

Fig. 1. The Eastern Bering Sea.

The annual cycle of sea ice coverage in the EBS directly influences ecosystem productivity. Winter winds that bring cold arctic air and ice from the north into the Bering Sea affect the extent of the annual sea ice formation in the EBS and the timing of sea ice breakup in the spring (Hunt et al., 2002, 2011; Stabeno et al., 2012). The extent of the winter sea ice influences the formation and structure of the summer "cold pool", a body of dense cold water (<2° C) that remains on the shallow shelf bottom after the ice retreats in the spring (**Fig. 2**). In "cold" years with extensive winter sea ice, the cold pool extends south to the Alaska Peninsula; in "warm" years it does not extend far beyond St Matthew Island, a difference of about 800 km. The cold pool influences spring and summer oceanographic conditions (e.g., stratification) as well as the distribution of species that may have different tolerances or preferences for the cold bottom water. Thus, food-web interactions can vary each year as predators and their prey respond differently to the extent and location of the cold pool (Mueter et al., 2011; Stabeno et al., 2012; Sigler et al., 2016).

Fig. 2. The annual extent of the cold pool of bottom water on the Eastern Bering Sea shelf from 2001-2017. Maps represent interpolated hydrographic observations and were developed by Carol Ladd (Siddon and Zador, 2017).

The EBS experiences shifts between consecutive years of predominantly warm or cold conditions (i.e., years typified by small or large cold pools, respectively), which provide contrast to evaluate the drivers of biological productivity (**Fig. 2**; Stabeno et al., 2012). While phytoplankton blooms occur regularly in the spring, the duration and timing of blooms, as well as the sizes of phytoplankton, vary substantially between warm and cold years. These divergent bloom characteristics, in turn, influence the size and energy content of zooplankton prey (Hunt et al., 2011). In general, cold years are typified by large phytoplankton, which support higher abundances of krill and larger species of copepods, which themselves become energy-rich prey for their fish predators, including pollock. In contrast, during warm years there are more small-sized species of copepods, which are not as energy-rich.

Feeding on energy-rich prey can improve fish condition and increase their overwinter survival rates. For example, when young pollock at the end of their first summer have high average energy content (a combination of energy density and fish weight), their overwinter survival is also higher (Siddon et al., 2017a; Heintz et al., 2013).

In 2012, the EBS experienced the coldest average bottom temperature (**Fig. 3**) and largest cold pool since 1999, which provided an extreme case to test the hypothesis that cold conditions favor young pollock (**Fig. 2**). During the cold summer, the spatial overlap between young pollock and their preferred zooplankton prey appeared high (Siddon et al., 2017b). However, the pollock were much smaller than average at the end of their first summer. While their energy density was high, as is typical in cold years, their small size contributed to a low average energy content per fish, which led to the prediction of poor overwinter survival (Heintz et al., 2013b). However, current estimates of the pollock stock suggest that this 2012 year class of pollock may in fact be one of the largest in the past three decades (**Fig. 4**). The 2012 year class now dominates the estimates of total pollock spawning biomass, which is currently at an overall high level and supports a large fishery quota (**Fig. 5**; Ianelli et al., 2016).
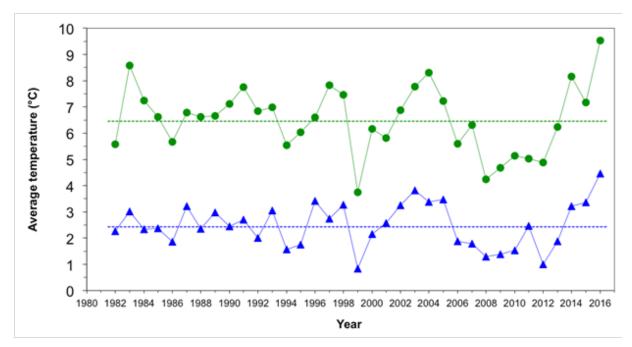

Fig. 3. Average summer surface (green dots) and bottom (blue triangles) water temperatures (°C) of the eastern Bering Sea shelf collected during the NOAA Fisheries summer bottom-trawl surveys. Dotted lines represent the time-series mean for 1982-2016. From Zador and Siddon, 2016.
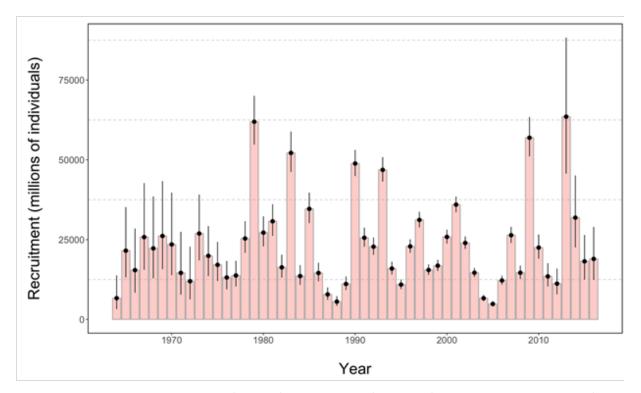
Fig. 4. Recruitment estimates (the number of age-1s) for Eastern Bering Sea pollock from the 2016 stock assessment for all years since 1964 (1963-2015 year classes). Error bars reflect 90% credible intervals based on model estimates of uncertainty From Ianelli et al., 2016.

The explanation for the surprisingly strong 2012 year class remains uncertain and is an active area of study. Better scientific understanding of how ecosystem components interact enables ecosystem science to inform fisheries management (Zador et al., 2017). For example, despite the current high EBS pollock stock size, the fisheries managers selected a more conservative catch limit than the maximum permissible in 2016 (Federal Register, 2017). The justification for this reduction included the recent warm environmental conditions; low abundances of age-1 and age-10 and older pollock; the anticipated poor survival of age-0 pollock; the continued decline in acoustic survey estimates of krill, an important prey; and the continued declines in northern fur seals, which prey upon pollock.

The current status of groundfish stocks in the EBS appear favorable overall. However, the longer-term effects of the recent, and record, warm years in the EBS will continue to be closely watched. Long-term climate projections for the EBS indicate significant warming of both surface and bottom summer temperatures, especially in the southern EBS shelf, as well as declines in sea ice extent in the winter and the extent and intensity of the cold pool. Concomitant shifts in productivity are anticipated; these shifts include declines in large zooplankton biomass, which may impact survival of groundfish species including pollock (Ortiz et al., 2016; Hermann et al., 2016). Multiple studies predict overall declines in pollock biomass in the EBS under future warming conditions (Ianelli et al., 2016b; Seung and Ianelli, 2016; Spencer et al., 2016).
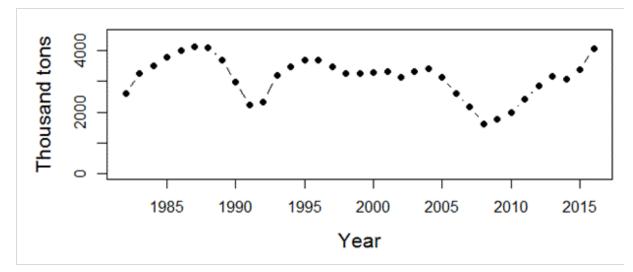
Fig. 5. Estimated Eastern Bering Sea female pollock spawning biomass. Biomass units are in thousands of tons. Data from Ianelli et al., 2016.

Projected effects in adjacent large marine ecosystems will likely differ from those in the EBS, based on inherent differences in geography, oceanography, and food webs. For example, the adjacent Aleutian Islands ecosystem encompasses a long chain of islands with extensive nearshore habitat, a narrow shelf, and abyssal waters to the north and the south. Local ecological communities typified by rockfish (*Sebastes* spp.) and sea otters (*Enhydra lutris*) will not be able to simply shift their distributions northward due to the absence of nearshore habitat. North of the EBS, continuing winter sea ice cover, in spite of less spring sea ice (due to earlier breakup), remains a barrier to ecosystem expansions. This can influence the scope for fisheries and fishing communities to adapt to climate change. For example, the ability of pollock fisheries to adapt to reduced productivity in the south EBS and northward shifting groundfish distributions may be limited by continued winter sea ice and existing fishery closure areas that limit northward expansion of the fishery. Thus, understanding ecological and socioeconomic implications of climate-driven changes requires ecosystem-specific understanding of mechanistic processes and species physiological threshold (Pörtner and Farrell, 2008) to project trends in species and environmental conditions.

References

Cheung, W. W. L., R. D. Brodeur, T. A. Okey, and D. Pauly, 2015: Projecting future changes in distributions of pelagic fish species of Northeast Pacific shelf seas. *Progress in Oceanography*, 130, 19-31. https://doi.org/10.1016/j.pocean.2014.09.003.

FAO, 2017: FAO Global Capture Production database updated to 2015 - Summary information. http://www.fao.org/3/a-br186e.pdf.

Federal Register, 2017: Final 2017 Overfishing Level (OFL), Acceptable Biological Catch (ABC), Total Allowable Catch (TAC), Initial TAC (ITAC), And CDQ Reserve Allocation Of Groundfish In The BSAI. Vol. 82, No. 37.

Fissel, B., M. Dalton, R. Felthoven, B. Garber-Yonts, A. Haynie, S. Kasperski, J. Lee, D. Lew, A. Santos, C. Seung, and K. Sparks, 2016: Stock Assessment and Fishery Evaluation Report for the Groundfish Fisheries of the Gulf of Alaska and Bering Sea/Aleutian Islands Area: Economic Status of the Groundfish Fisheries Off Alaska, 2015. Stock Assessment and Fishery Evaluation Report, North Pacific Fishery Management Council, 605 W 4th Ave, Suite 306, Anchorage, AK 99501.

Haynie, A., and L. Pfeiffer, 2013: Climatic and economic drivers of the Bering Sea walleye pollock (*Theragra chalcogramma*) fishery: implications for the future. *Canadian Journal of Fisheries and Aquatic Science*, 70(April), 841-853. https://doi.org/dx.doi.org/10.1139/cjfas-2012-0265.

Heintz, R. A., E. Farley, and E. C. Siddon, 2013b: Fall condition of YOY predicts recruitment of age-1 walleye pollock. In: *Ecosystem Considerations 2013, Stock Assessment and Fishery Evaluation Report*, North Pacific Fishery Management Council, 605 W 4th Ave, Suite 306, Anchorage, AK 99501.

Heintz, R. A., E. C. Siddon, E. V. Farley Jr., and J. M. Napp, 2013: Correlation between recruitment and fall condition of age-0 walleye pollock (*Theragra chalcogramma*) from the eastern Bering Sea under varying climate conditions. *Deep Sea Res Part II: Top Stud Oceanogr,* 94, 150-156.

Hermann, A. J., G. A. Gibson, N. A. Bond, E. N. Curchitser, K. Hedstrom, W. Cheng, M. Wang, E. D. Cokelet, and P. J. Stabeno, 2016: Projected future biophysical states of the Bering Sea. *Deep Sea Research Part II: Topical Studies in Oceanography*, 134, 30-47.

Hunt, Jr., G. L., P. Stabeno, G. Walters, E. Sinclair, R. D. Brodeur, J. M. Napp, and N. A. Bond, 2002: Climate change and control of the southeastern Bering Sea pelagic ecosystem. *Deep Sea Research Part II: Topical Studies in Oceanography*, 49(26), 5821-5853.

Hunt, Jr., G. L., K. O. Coyle, L. B. Eisner, E. V. Farley, R. A. Heintz, F. Mueter, J. M. Napp, J. E. Overland, P. H. Ressler, S. Salo, and P. J. Stabeno, 2011: Climate impacts on eastern Bering Sea foodwebs: a synthesis of new data and an assessment of the Oscillating Control Hypothesis. *ICES Journal of Marine Science*, 68(6), 1230-1243.

Ianelli, J., K. K. Holsman, A. E. Punt, and et al., 2016b: Multi-model inference for incorporating trophic and climate uncertainty into stock assessments. *Deep Sea Research Part II: Topical Studies in Oceanography*, 134, 379-389.

Ianelli, J. N., T. Honkalehto, S. Barbeaux, B. Fissel, and S. Kotwicki, 2016: Assessment of the walleye pollock stock in the Eastern Bering Sea, Stock Assessment and Fishery Evaluation Report, North Pacific Fishery Management Council, 605 W 4th Ave, Suite 306, Anchorage, AK 99501.

Mueter, F. J., N. A. Bond, J. N. Ianelli, and A. B. Hollowed, 2011: Expected declines in recruitment of walleye pollock (*Theragra chalcogramma*) in the eastern Bering Sea under future climate change. *ICES Journal of Marine Science*, 68(6), 1284-1296.

Ortiz, I., K. Aydin, A. J. Hermann, G. A. Gibson, A. E. Punt, F. K. Wiese, and C. Boyd, 2016: Climate to fish: Synthesizing field work, data and models in a 39-year retrospective analysis of seasonal processes on the eastern Bering Sea shelf and slope. *Deep-Sea Research Part II: Topical Studies in Oceanography*, 134, 390-412. https://doi.org/10.1016/j.dsr2.2016.07.009.

Pinsky, M. L., B. Worm, M. J. Fogarty, J. L. Sarmiento, and S. A. Levin, 2013: Marine taxa track local climate velocities. *Science*, 341(6151), 1239-1242. https://doi.org/10.1126/science.1239352.

Pörtner, H. O., and A. P. Farrell, 2008: Physiology and climate change. *Science*, 690-692.

Seung, C., and J. Ianelli, 2016:. Regional economic impacts of climate change: a computable general equilibrium analysis for an Alaskan fishery. *Natural Resource Modeling*, 29, 289-333.

Siddon, E. C., J. T. Duffy-Anderson, K. L. Mier, M. S. Busby, and L. B. Eisner, 2017a: Seasonal, interannual, and spatial patterns of community composition over the eastern Bering Sea shelf in cold years. Part II: ichthyoplankton and juvenile fish, *ICES Journal of Marine Science*, fsx123, https://doi.org/10.1093/icesjms/fsx123.

Siddon, E. C., et al., 2017b: (tentative title) Spatial overlap of age-0 pollock and their zooplankton prey. In: *Ecosystem Considerations 2017: Status of the Eastern Bering Sea Marine Ecosystem*, Stock Assessment and Fishery Evaluation Report, North Pacific Fishery Management Council, 605 W 4th Ave, Suite 306, Anchorage, AK 99501.

Siddon, E., and S. Zador, 2017: In: *Ecosystem Considerations 2017: Status of the Eastern Bering Sea Marine Ecosystem*, Stock Assessment and Fishery Evaluation Report, North Pacific Fishery Management Council, 605 W 4th Ave, Suite 306, Anchorage, AK 99501.

Sigler, M. F., J. M. Napp, P. J. Stabeno, R. A. Heintz, M. W. Lomas, and G. L. Hunt, 2016: Variation in annual production of copepods, euphausiids, and juvenile walleye pollock in the southeastern Bering Sea. *Deep Sea Research Part II: Topical Studies in Oceanography*, 134, 223-234.

Spencer, P. D., K. K. Holsman, S. Zador, et al., 2016: Modelling spatially dependent predation mortality of eastern Bering Sea walleye pollock, and its implications for stock dynamics under future climate scenarios. *ICES Journal of Marine Science*, 73, 1330-1342.

Stabeno, P. J., N. B. Kachel, S. E. Moore, J. M. Napp, M. Sigler, A. Yamaguchi, and A. N. Zerbini, 2012: Comparison of warm and cold years on the southeastern Bering Sea shelf and some implications for the ecosystem. *Deep Sea Research Part II: Topical Studies in Oceanography*, 65, 31-45.

Stabeno, P. J., J. D. Schumacher, and K. Ohtani, 1999: The physical oceanography of the Bering Sea. In: Loughlin, T. R., Ohtani, K. (Eds.), *Dynamics of the Bering Sea: A Summary of Physical, Chemical, and Biological Characteristics, and a Synopsis of Research on the Bering Sea*, North Pacific Marine Science Organization (PICES), University of Alaska Sea Grant, AK-SG-99-03, Fairbanks, Alaska, USA, pp.1-28.

Zador, S., and E. Siddon, 2016: Ecosystem Considerations 2016: Status of the Eastern Bering Sea Marine Ecosystem, Stock Assessment and Fishery Evaluation Report, North Pacific Fishery Management Council, 605 W 4th Ave, Suite 306, Anchorage, AK 99501.

Zador, S. G., K. K. Holsman, K. Y. Aydin, and S. K. Gaichas, 2017: Ecosystem considerations in Alaska: the value of qualitative assessments. *ICES Journal of Marine Science*, 74(1), 421-430.

November 20, 2017

Wildland Fire in High Latitudes

A. York[1], U. Bhatt[2], R. Thoman[3], R. Ziel[1]

[1]Alaska Fire Science Consortium, International Arctic Research Center, University of Alaska, Fairbanks, AK, USA

[2]Geophysical Institute, University of Alaska, Fairbanks, AK, USA

[3]National Weather Service, Alaska Region, Anchorage, AK, USA

Highlights

- High latitude fire regimes appear to be responding rapidly to environmental changes associated with a warming climate; although highly variable, area burned has increased over the past several decades in much of Boreal North America.
- Most acreage burned in high latitude systems occurs during sporadic periods when lightning ignitions coincide with warm and dry weather that cures vegetation and elevates fire danger.
- Under a range of climate change scenarios, analyses using multiple approaches project significant increases (up to four-fold) in area burned in high latitude ecosystems by the end of the 21st century.

Despite the low annual temperatures and short growing seasons characteristic of northern ecosystems, wildland fire affects both boreal forest (the broad band of mostly coniferous trees that generally stretches across the area north of the July 13° C isotherm in North America and Eurasia, also known as Taiga) and adjacent tundra regions. In fact, fire is the dominant ecological disturbance in boreal forest, the world's largest terrestrial biome. Fire disturbance affects these high latitude systems at multiple scales, including direct release of carbon through combustion (Kasischke et al., 2000) and interactions with vegetation succession (Mann et al., 2012; Johnstone et al., 2010), biogeochemical cycles (Bond-Lamberty et al., 2007), energy balance (Rogers et al., 2015), and hydrology (Liu et al., 2005). About 35% of global soil carbon is stored in tundra and boreal systems (Scharlemann et al., 2014) that are potentially vulnerable to fire disturbance (Turetsky et al., 2015). This brief report summarizes evidence from Alaska and Canada on variability and trends in fire disturbance in high latitudes and outlines how short-term fire weather conditions in these regions influence area burned.

Beyond immediate threats to lives and property, wildland fire has multiple impacts on northern environments and residents. Smoke can be widespread and compromise health, particularly in vulnerable populations (Reid et al., 2016). Wildfire smoke can also limit visibility and constrain aviation operations, including those supporting fire suppression and detection. Black carbon, derived from wildfires, is known to travel considerable distances and accelerate surface melting and thawing of snow and ice (Thomas et al., 2017). Removal of the surface organic layer by combustion has been shown to initiate the development of thermokarst in both boreal and tundra soils, which are rich in permafrost (Jorgenson et al., 2010; Jones et al., 2015).

Climate is a dominant control of fire activity in both boreal and tundra ecosystems. The relationship between climate and fire is strongly nonlinear, with the likelihood of fire occurrence within a 30-year period much higher where mean July temperatures exceed 13.4° C (56° F) (Young et al., 2017). High latitude fire regimes appear to be responding rapidly to recent environmental changes associated with the warming climate. Although highly variable, area burned has increased over the past several decades in much of boreal North America (Kasischke and Turetsky, 2006; Gillett et al., 2004). Since the early 1960s, the number of individual fire events and the size of those events has increased, contributing to more frequent large fire years in northwestern North America (Kasischke and Turetsky, 2006). **Figure 1** shows annual area burned per year in Alaska (a) and Northwest Territories (b) since 1980, including both boreal and tundra regions.

Fig. 1. Annual area burned per year in Alaska (a) and Northwest Territories (b) since 1980, including both boreal and tundra regions. Note that high fire years are not coincident in these sub-regions, indicating the importance of local weather conditions. "Normal" is the middle tercile (33rd-66th percentiles) of the fitted distribution.

Recent large fire seasons in high latitudes include 2014 in the Northwest Territories, where 385 fires burned 8.4 million acres, and 2015 in Alaska, where 766 fires burned 5.1 million acres (**Figs. 1** & **2**)—more than half the total acreage burned in the US (NWT, 2015; AICC, 2015). Multiple northern communities have been threatened or damaged by recent wildfires, notably Fort McMurray, Alberta, where 88,000 people were evacuated and 2400 structures were destroyed in May 2016. Examples of recent significant tundra fires include the 2007 Anaktuvuk River Fire, the largest and longest-burning fire known to have occurred on the North Slope of Alaska (256,000 acres), which initiated widespread thermokarst development (Jones et al., 2015). An unusually large tundra fire in western Greenland in 2017 received considerable media attention.

Fig. 2. MODIS false color image of Alaska on September 1, 2015, showing burn scars, mostly from the 2015 fire season. Image from NASA Earth Observatory.
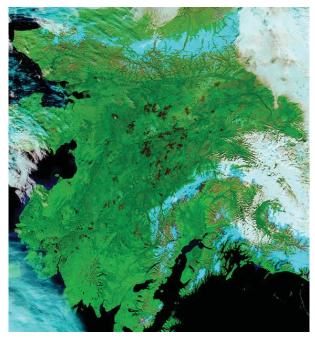
Large fire events such as these require the confluence of receptive fuels that will promote fire growth once ignited, periods of warm and dry weather conditions, and a source of ignition—most commonly, convective thunderstorms that produce lightning ignitions. High latitude ecosystems are characterized by unique fuels—in particular, fast-drying beds of mosses, lichens, resinous shrubs, and accumulated organic material (duff) that underlie dense, highly flammable conifers. These understory fuels cure rapidly during warm, dry periods with long daylight hours in June and July. Consequently, extended periods of drought are not required to increase fire danger to extreme levels in these systems.

Lightning has historically been responsible for the majority of acres burned in high latitudes, as lightning-ignited fires tend to occur in more remote locations and thus are subject to lower levels of suppression than human-started incidents. Veraverbeke et al. (2017) recently showed that lightning ignitions have increased in boreal North America since 1975 and largely drove the extreme 2014 Northwest Territories and 2015 Alaska fire seasons. In addition, Partain et al. (2016) found that human-induced climate change, manifested as a combination of high surface temperatures, low relative humidity, and low precipitation, increased the likelihood of the extremely dry fuel conditions seen in Alaska in 2015 by 34-60%.

Most acreage burned in high latitude systems occurs during sporadic periods of high fire activity; 50% of the acreage burned in Alaska from 2002 to 2010 was consumed in just 36 days (Barrett et al., 2016). **Figure 3** shows cumulative acres burned in the four largest fire seasons in Alaska since 1990 (from **Fig. 1**) and illustrates the varying trajectories of each season. Some seasons show periods of rapid growth during unusually warm and dry weather (2004, 2009, 2015), while others (2004 and 2005) were prolonged into the fall in the absence of season-ending rain events. In 2004, which was Alaska's largest wildfire season at 6.6 million acres, the trajectory was characterized by both rapid mid-season growth and extended activity into September. These different pathways to large fire seasons demonstrate the importance of intraseasonal weather variability and the timing of dynamical features. As another example, although not large in total acres burned, the 2016 wildland fire season in Alaska was more than 6 months long, with incidents requiring response from mid-April through late October (AICC, 2016).

Fig. 3. Averaged daily cumulative acres burned for specific recent above-normal fire years in Alaska compared to the climatological 25th and 75th percentile (1994-2015) levels. The other above-75th percentile years of 1997 and 2002 are not shown for clarity because they lie close to the 75th percentile. (From Partain et al., 2016).

The snow-free season is increasing by approximately 5 days per decade in Alaska (Liston and Hiemstra, 2011), and the state's fire management agencies advanced the statutory date of fire season from May 1 to April 1 in 2006 to better prepare for early events. In addition to tracking long-term trends and the impacts of a shifting climate, managers in Alaska and Canada must prepare for day-to-day variability in threats to its dispersed population with very limited resources. The Canadian Forest Fire Weather Index (FWI) System is used on a daily basis to estimate the spatial and temporal distribution of wildfire potential from observed and forecasted weather conditions (Lawson and Armitage, 2008). Among its indices, the Buildup Index (BUI), based on cumulative scoring of daily temperature, relative humidity, and precipitation, represents seasonal variability in fuel availability and flammability (**Fig. 4**). A threshold of 80 has been identified as a critical indicator of fire growth potential throughout the fire-prone landscape (Ziel et al., 2015).

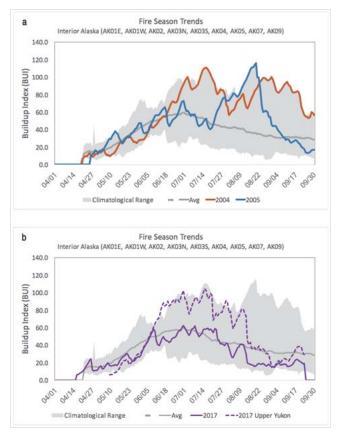**Fig. 4.** Average (grey line) and climatological range (grey shading) of Buildup Index (BUI) in Alaska's Boreal Interior for 1994-2017, compared to 2004 (4a, red line), 2005 (4a, blue line) and 2017 (4b, purple line), and for the Predictive Service Area AK02 (Upper Yukon and surrounding uplands) in 2017 (4b, dashed purple line). While the overall average for 2017 mirrors the historic average trend, there is a significant departure in the Upper Yukon Zone, where the majority of the acres burned in the state in 2017.

Figure 4a shows trends in BUI over selected seasons (2004 and 2005) in interior Alaska compared to the climatological range and average, derived from combined records from 116 surface observing locations from 1994-2017. Values for BUI in 2004 were elevated for a prolonged period in late June and July, and in both 2004 and 2005 reached extreme levels into August and September, consistent with the well above normal area burned late in those seasons (**Figs. 1a** and **3**). In contrast, BUI values in 2015 (data not shown) were elevated in early to mid-season, coincident with the relatively brief period of extremely rapid fire growth, sparked by abundant lightning ignitions, seen in June and early July (**Fig. 3**).

In 2017, the typical acreage burned in Alaska (**Fig. 1**) was reflected by a fairly normal BUI trend across the boreal region that essentially paralleled the climatological average (**Fig. 4b**). However, it is noteworthy to reflect on how disproportionately the impact of a "normal" season can fall on specific areas in a landscape this large. For instance, while there were no significant peaks in the overall trend, local conditions in the Upper Yukon zone in northeast Alaska were significantly warmer and drier. Consistent with the Upper Yukon BUI trend (**Fig. 4b**), the season was extended and fairly severe in that large corner of the state, with periods of high fire danger (BUI ≥ 80) from mid-June into mid-August. More than 410,000 acres (63% of the 2017 Alaska total) were burned in the Upper Yukon area during this period (AICC, 2017).

Under a range of climate change scenarios, analyses using multiple approaches project significant increases (up to four-fold) in area burned in high latitude ecosystems by the end of the 21st century (French et al., 2015; Young et al., 2017; Yue et al., 2015, and references therein). In addition, lightning frequency is projected to increase by 12+/-5% per °C of warming in the contiguous U.S. (Romps et al., 2014), and may increase correspondingly in high latitudes. Because specific fire events depend on multiple interacting factors, the resulting changes in high latitude fire regimes will vary greatly over space and time, but all evidence indicates that northern ecosystems will become increasingly susceptible to burning.

References

Alaska Interagency Coordination Center (AICC), 2015: 2015 Fall Fire Review Statistics Summary. https://fire.ak.blm.gov/content/aicc/stats/Alaska%20Fire%20Numbers.pdf.

Alaska Interagency Coordination Center (AICC), 2016: 2016 Alaska Fire Season. https://fire.ak.blm.gov/content/aicc/Statistics%20Directory/Previous%20Years%20Fall%20Fire%20Review%20Handouts/2016%20Fire%20Data/2016%20Alaska%20Fire%20Se

Alaska Interagency Coordination Center (AICC), 2017: Situation Report. https://fire.ak.blm.gov/content/aicc/sitreport/current.pdf.

Barrett, K., T. Loboda, A. D. McGuire, H. Genet, E. Hoy, and E. Kasischke, 2016: Static and dynamic controls on fire activity at moderate spatial and temporal scales in the Alaskan boreal forest. *Ecosphere*, 7(11), e01572, doi: 10.1002/ecs2.1572.

Bond-Lamberty, B., S. D. Peckham, D. E. Ahl, and S. T. Gower, 2007: Fire as the dominant driver of central Canadian boreal forest carbon balance. *Nature*, 450(7166), 89-92.

French, N. H. F., L. K. Jenkins, T. V. Loboda, M. Flannigan, R. Jandt, L. L. Bourgeau-Chavez, and M. Whitley, 2015: Fire in arctic tundra of Alaska: past fire activity, future fire potential, and significance for land management and ecology. *International Journal of Wildland Fire*, http://dx.doi.org/10.1071/WF14167.

Gillett, N. P., A. J. Weaver, F. W. Zwiers, and M. D. Flannigan, 2004: Detecting the effect of climate change on Canadian forest fires. *Geophysical Research Letters*, 31, L18211.

Johnstone, J. F., T. N. Hollingsworth, F. S. Chapin, and M. C. Mack, 2010: Changes in fire regime break the legacy lock on successional trajectories in Alaskan boreal forest. *Global Change Biology*, 16, 1281-1295, doi: 10.1111/j.1365-2486.2009.02051.x.

Jones, B., G. Grosse, C. D. Arp, E. A. Miller, L. Liu, D. J. Hayes, and C. F. Larsen, 2015: Recent Arctic tundra fire initiates widespread thermokarst development. *Scientific Reports*, 5. 15865, doi: 10.1038/srep15865.

Jorgenson, M. T., V. E. Romanovsky, J. Harden, Y. Shur, J. O'Donnell, E. A. G. Schuur, M. Kanevskiy, and S. Marchenko, 2010: Resilience and vulnerability of permafrost to climate change. *Canadian Journal of Forest Research*, 2010, 40, 7, 1219-1236. https://doi.org/10.1139/X10-060.

Kasischke, E. S., K. P. O'Neill, N. H. F. French, and L. L. Bourgeau-Chavez, 2000: Controls on patterns of biomass burning in Alaskan boreal forests, in *Fire, Climate Change, and Carbon Cycling in the Boreal Forest*, pp 173-196, Springer: New York.

Kasischke, E. S., and M. R. Turetsky, 2006: Recent changes in the fire regime across the North American boreal region-spatial and temporal patterns of burning across Canada and Alaska. *Geophysical Research Letters*, 33, L09703.

Lawson, B..D., and O. B. Armitage,2008: Weather guide for the Canadian Forest Fire Danger Rating System. Nat. Resour. Can., Can. For. Serv., North. For. Cent., Edmonton, AB.

Liston, G. E. and C. A. Hiemstra, 2011: The changing cryosphere: Pan-Arctic snow trends (1979-2009). *Journal of Climate*, 24, 5691-5712.

Liu, H., J. T. Randerson, J. Lindfors, and F. S. Chapin, 2005: Changes in the surface energy budget after fire in boreal ecosystems of interior Alaska: An annual perspective. *Journal of Geophysical Research*, 110(D13), doi: 10.1029/2004JD005158.

Mann, D. H., T. S. Rupp, M. A. Olson, and P. A. Duffy, 2012: Is Alaska's Boreal Forest Now Crossing a Major Ecological Threshold? *Arctic, Antarctic, and Alpine Research*, 44, 3, 319-331. https://doi.org/10.1657/1938-4246-44.3.319.

Northwest Territories Department of Environment and Natural Resources (NWT), 2015: 2014 NWT Fire Season Review Report. http://www.enr.gov.nt.ca/sites/enr/files/web_pdf_fmd_2014_fire_season_review_report_4_may_2015.pdf.

Partain, J. L., S. Alden, U. S. Bhatt, P. A. Bieniek, B. R. Brettschneider, R. T. Lader, P. Q. Olsson, T. S. Rupp, H. Strader, R. L. Thoman, J. E. Walsh, A. D. York, and R. H. Ziel, 2016: An assessment of the role of anthropogenic climate change in the Alaska fire season of 2015 [in "Explaining Extremes of 2015 from a Climate Perspective"]. *Bulletin of the American Meteorological Society*, 97 (12), S14-S18, doi: 10.1175/BAMS-D-16-0149.1.

Reid, C.E., M. Brauer, F. H. Johnston, M. Jerrett, J. R. Balmes, and C. T. Elliott, 2016: Critical review of health impacts of wildfire smoke exposure. *Environmental Health Perspectives*, 124, 1334-1343, http://dx.doi.org/10.1289/ehp.1409277.

Rogers, B. M., A. J. Soja, M. L. Goulden, and J. T. Randerson, 2015: Influence of tree species on continental differences in boreal fires and climate feedbacks. *Nature Geoscience*, 8(3), 228-234, doi: 10.1038/ngeo2352.

Romps, D. M., J. T. Seeley, D. Vollaro, and J. Molinari, 2014: Projected increase in lightning strikes in the United States due to global warming. *Science*, 346, 851-854.

Scharlemann, J. P., E. V. Tanner, R. Hiederer, and V. Kapos, 2014: Global soil carbon: understanding and managing the largest terrestrial carbon pool. *Carbon Management*, 5, 81-91.

Thomas, J. L., et al., 2017: Quantifying black carbon deposition over the Greenland ice sheet from forest fires in Canada. *Geophysical Research Letters*, 44, 7965-7974, doi: 10.1002/2017GL073701.

Turetsky, M., B. Benscoter, S. Page, G. Rein, G. R. van der Werf, and A. Watts, 2015. Global vulnerability of peatlands to fire and carbon loss. *Nature Geoscience,* 8(1), 11-14,. doi: 10.1038/NGEO2325.

Veraverbeke, S., B. M. Rogers, M. L. Goulden, R. R. Jandt, C. E. Miller, E. B. Wiggins, and J. T. Randerson, 2017: Lightning as a major driver of recent large fire years in North American boreal forests. *Nature Climate Change*, 7, 529-534, doi: 10.1038/nclimate3329.

Young, A. M., P. E. Higuera, P. A. Duffy, and F. S. Hu, 2017: Climatic thresholds shape northern high-latitude fire regimes and imply vulnerability to future climate change. *Ecography*, 40, 606-617, http://dx.doi.org/10.1111/ecog.02205.

Yue, X., L. J. Mickley, J. A. Logan, R. C. Hudman, M. V. Martin, and R. M. Yantosca, 2015: Impact of 2050 climate change on North American wildfire: consequences for ozone air quality. *Atmospheric Chemistry and Physics*, 15, 10033-10055, doi: 10.5194/acp-15-10033-2015.

Ziel, R. H., et al., 2015: Modeling fire growth potential by emphasizing significant growth events: characterizing climatology of fire growth days in Alaska's boreal forest. 11th Symp. on Fire and Forest Meteorology, Minneapolis MN, *Amer. Meteor. Soc.*, 1.2. [Available online at https://ams.confex.com/ams/11FIRE/webprogram/Paper272864.html.]

December 5, 2017

Paleoceanographic Perspectives on Arctic Ocean Change

E. Osborne[1], T. Cronin[2], J. Farmer[3]

[1]NOAA Arctic Research Program, Office of Oceanic and Atmospheric Research, Silver Spring, MD, USA

[2]U.S. Geological Survey, Reston, VA, USA

[3]Princeton University - Department of Geosciences, Princeton, NJ, USA

Highlights

- High-resolution Arctic paleo-reconstructions indicate that the magnitude and pace of the 21st century sea-ice decline and surface ocean warming is unprecedented in the last 1,500 years.
- Regions of year-round sea ice likely persisted over much of the past 350,000 years with intermittent ice-free periods until 5,000 years ago, when modern sea ice conditions developed.
- Paleo-reconstructions indicate that Arctic sea ice extent correlates broadly with temperatures and atmospheric CO_2 concentrations over geologic time.

The Arctic Ocean is presently experiencing changes in ocean temperature and sea ice extent that are unprecedented in the observational time period (satellite observations: 1979-Present). To provide context for the current changes, scientists turn to paleo records of past climate to document and study natural variability in the Arctic system. Paleoceanographic records that extend limited Arctic instrumental measurements are central to improving our understanding of sea ice dynamics and ocean warming and for enhancing the predictive capability of models. By coupling paleoceanographic records with modern observations, scientists can also contextualize the rate and magnitude of modern change with the deep past.

Proxy Techniques to Investigate Past Ocean Temperature and Sea Ice

Paleoceanographers reconstruct past climate using proxies, or surrogates of past climate variables, preserved in geologic records that have the potential to span millions of years (**Table 1**). Proxy records are derived from biological, physical or chemical measurements that, for example, can be made using sediment cores (lake or marine), ice cores, or fossil calcium carbonate shells (e.g., corals, foraminifera, ostracodes). Some paleoclimate archives contain relatively direct measurements, such as atmospheric gas concentrations (e.g., CO_2, CH_4) trapped in bubbles recovered from Antarctic, Greenland and Alpine ice cores. Others can be less direct, such as measuring marine microfossil shell geochemistry to reconstruct past ocean temperature. Proxies are rigorously tested using a number of methods and are often compared to instrumental records to develop an understanding of the proxy.

When proxies are applied to core sediment records, they produce reconstructions with variable time resolution based on the study region's sedimentation rate. For example, sediment cores collected from the central deep-Arctic basin, where sediments accumulate at extremely low rates, have the potential to produce very long-term but low time resolution records. Alternatively, marginal Arctic seas have much higher sedimentation rates due to high primary biological productivity and terrigenous (i.e., derived from land erosion) sediment influx, which facilitates the preservation of proxies in sediments with greater time resolution. Paleoceanographers depend on combinations of

Table 1. Arctic paleoceanographic proxies and important relative references that are included in the studies described in this essay.

Proxy		Indicator Type	Explanation
Ice Rafted Debris		Sea Ice, Glaciers, Ice Sheets	Sediment-laden ice from continental margins drops terrigenous (land-based) material from melting ice and deposited on the seafloor
Bathymetry		Ice extent	Seabed features can be used to determine the extent and thickness of ice sheets and ice shelves that were large enough to scour the seafloor
Microfossil Abundance			Microscopic shell-building organisms that either float in the water column (planktic) or live on the seafloor (benthic) whose fossil remains are preserved in seafloor sediments.
Ostracodes		Sea Ice, Temperature	Bivalved Crustacea that secrete a pair of symmetrical calcium carbonate valves. They are found in a range of fresh and marine environments and can be planktic or benthic.
Foraminifera		Temperature, Seawater Chemistry	Single-celled organisms that secrete calcium carbonate shells (tests). They are distributed throughout the global ocean and can be planktic or benthic.
Diatoms		Sea Ice, Temperature	Photosynthetic algae that build siliceous skeletons (frustules) that are found in fresh and marine environments. They can be planktic or benthic and some species are suited to live within sea ice.
Dinoflagellate cysts		Sea Ice, Temperature	Many but not all are photosynthetic planktic organisms. They are often symbionts (e.g. corals or foraminifera). The dormant spore-life state (cysts) are excellently preserved in sediments
Geochemistry			The elemental and isotopic composition of foraminifera and ostracodes reflect changes in local environmental conditions. Species-specific effects require unique species proxy calibrations.
Mg/Ca		Temperature	Mg is substituted into the calcium carbonate lattice of microfossil shells as a function of temperature, with higher Mg/Ca coinciding with warmer temperatures
$\delta^{18}O$		Temperature, Global Ice Volume, Salinity	The fractionation of oxygen-16 and -18 depends on seawater temperature and global volume of terrestrial ice.
Biomarkers		Sea Ice	The concentration of a lipid biomarker, IP25, exclusively produced by sea ice dwelling diatoms in sediment organic matter is used to reconstruct extent and concentration of sea ice

high- and low-resolution records to distinguish short- and long-term changes and processes. To further increase the confidence of proxy reconstructions, paleoceanographers often develop multi-proxy records; in these records, more than one proxy technique is used to reconstruct climate variables.

Arctic Paleotemperature and Sea Ice of the Geologic Past

Large seasonal variability of sea ice extent, particularly within marginal seas, is a key characteristic of the Arctic Ocean today. Over geological time, paleoceanographic reconstructions indicate the Arctic has experienced massive sea ice fluctuations from nearly completely ice-free to permanent ice-covered conditions. Much of the understanding of deep-time for the Arctic Ocean has been derived from the first and only successful scientific drilling expedition near the North Pole, Arctic Coring Expedition (ACEX; Integrated Ocean Discovery Program Expedition 302; **Fig. 1**), in the permanently ice-covered central Arctic (Lomonosov Ridge). The appearance of ice-rafted debris (IRD) and sea-ice dependent diatoms (*Synedropsis* spp.) in the >400 meters of Arctic marine sediments recovered from ACEX indicate the first Arctic sea ice formed approximately 47 million years ago in the central Arctic (St. John, 2008; Stickley et al., 2009). Global atmospheric CO_2 concentration and paleotemperature

records indicate that the development of Arctic sea ice coincided with a period of global climate cooling during the middle Eocene (**Fig. 2**). This transition in global climate is referred to as the shift from Early Cenozoic greenhouse (warm/high CO_2) to Late Cenozoic icehouse (cool/low CO_2) conditions. The development of year-round (i.e., perennial) sea ice at the North Pole, similar to conditions that exist today, is evident in sediment records as early as 14-18 million years ago (Darby, 2008). These geologic records suggest that transitions in sea ice cover occur over many millennia and often vary in concert with the waxing and waning of circum-Arctic ice sheets and long-term fluctuations in temperature and atmospheric CO_2 concentrations (Stein et al., 2012; Jakobsson et al., 2014 for a review).

Scientists believe that of the five major oceans, the Arctic experienced the most dramatic environmental change through its Quaternary (2.6 million years ago to present) history. During Quaternary glacial periods, vast glacial ice masses expanded across the entire Arctic Ocean drawing down global sea level, exposing the Arctic's broad

Fig. 1. International Bathymetric Chart of the Arctic Ocean (IBCAO) indicating the core locations of the studies included in this synthesis. Central Basin/Ridge Cores: St. John (2008), Stickley et al. (2009), Darby (2008), Polyak et al. (2013), Cronin et al.(2013). Shelf Cores: Stein et al. (2017), Polyak et al. (2016), Müller et al. (2012), Hörner et al. (2016), Vare et al. (2009), Spielhagen et al. (2011). Not included in figure: Data compilations from Kinnard et al. (2011) and McKay and Kaufman (2014).

Fig. 2. Global bottom water temperature and atmospheric CO_2 records spanning the last 60 million years plotted with major events in Northern Hemisphere sea ice development. Paleotemperature reconstructions are derived from global compilations of benthic foraminifera oxygen isotopic composition. Paleo-CO_2 estimates are derived from a number of proxy techniques from globally distributed recor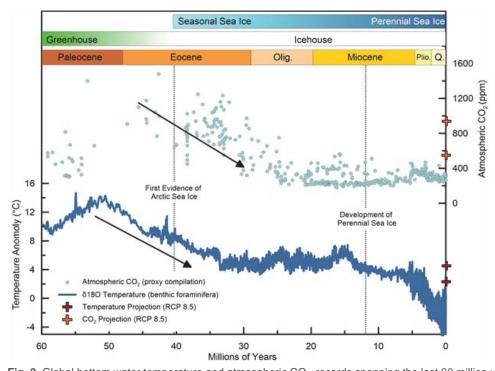ds (Compilation: Beerling and Royer, 2011 (see for dataset references); Zhang et al., 2013; Anagnostou et al., 2016). The red and orange (+) symbols indicate the projected global temperature anomaly and atmospheric CO_2 concentrations by the year 2050 and 2100 based on a "business-as-usual" scenario 8.5 from the 2013 IPCC AR5 report.

continental shelves and sometimes restricting the exchange between the Arctic and other global oceans. These vast glacial sea-based ice masses, also referred to as ice shelves, developed in concert with the growth of land-based ice sheets. Due to limited preservation of physical evidence, these ice shelves and their connection to circum-Arctic terrestrial ice sheets have been an enigmatic feature of Arctic glacial history. The existence of such ice conditions has been debated since the late 1800s, when a thick floating Arctic ice mass was first proposed. Recently, a geophysical study using multibeam bathymetry allowed researchers to map ice scouring and glacial landforms on the seafloor to constrain the extent and thickness of glacial ice shelves for the first time. This study concluded that a 1-km thick ice shelf covered much of the central Arctic during an extremely strong glacial period 140,000 to 160,000 years ago (Jakobsson et al., 2016). It is estimated that the volume of this particular glacial ice shelf is seven times greater than the total combined volume of all ice shelves on Earth today.

Multi-proxy records of ostracode and foraminifera microfossil assemblages and lithological changes within sediment cores collected on the Northwind and Mendeleev ridges in the western region of the central Arctic were used to reconstruct sea ice variability over the last one million years (**Fig. 1**). These records indicate that, during this period, perennial sea ice existed as early as 800,000 years ago in the high latitudes of the western Arctic and became a dominant feature 400,000 years ago (Polyak et al., 2013; Cronin et al., 2013). However, it is important to note ice-free conditions have been recorded during this period (e.g., Cronin et al., 2010). These reconstructions also suggest that periods of diminished sea ice in the western Arctic are directly related to enhanced inflow of

Pacific water into the central basin (Polyak et al., 2013). In contrast to the western Arctic records, eastern Arctic paleo-records indicate considerably later formation of sea ice (approximately 190,000 years ago; O'Regan et al., 2010). Given that the present-day sea-ice decline is most pronounced in the western Arctic, such regional variability is not surprising, and likely relates to varying inflow of Pacific and Atlantic waters to the Arctic (e.g., Spielhagen et al., 2011; Woodgate et al., 2010).

These records also indicate that over the past tens to hundreds of thousands of years, Arctic sea-ice cover was chiefly governed by ice-age climate cycles (Marzen et al., 2016; Cronin et al., 2010, 2013; Polyak et al., 2013) and also modulated by changes in solar insolation (the amount of solar radiation that reaches the Earth's surface), ice sheet and ice shelf configuration, atmospheric CO_2 concentrations, and inflowing Atlantic and Pacific waters (e.g., Stein et al., 2012).

Arctic Paleotemperature and Sea Ice: The last 10,000 Years

The Holocene interglacial period (11,700 years ago to present) represents the most recent stable warm period, which began after the transitional period of deglaciation (19,000-11,700 years ago). Holocene records of Arctic sea ice extent indicate considerable spatial and temporal variability over the last 10,000 years, including seasonally ice-free periods in various regions from 6,000 to 10,000 years ago when solar insolation in the Arctic was strongest (Polyak et al., 2010; Müller et al., 2012). For many parts of the Arctic, the modern (prior to anthropogenic forcing) perennial sea-ice cover did not fully develop until the latter half of the Holocene, about 5,000 years ago (Darby et al., 2006).

Rapid sediment accumulation in Arctic marginal seas allows for a detailed, higher-resolution history of sea ice variability to be obtained for the Holocene. High-resolution IP_{25} biomarker (**Table 1**) records from the Chukchi and East Siberian seas indicate that sea ice concentrations were controlled not only by decreasing insolation, but also by the fraction of Pacific water delivered via the Bering Strait (Stein et al., 2017; Polyak et al., 2016). Records of IP_{25} from the Fram Strait (Müller et al., 2012), the Laptev Sea (Horner et al., 2016) and the Canadian Arctic Archipelago (Vare et al., 2009) agree with the long-term trends recorded in the Chukchi and Eastern Siberian seas, demonstrating that there was a circum-Arctic Holocene expansion of sea ice in the marginal seas. Lithologic, geochemical and microfossil records from the Fram Strait also indicate regional variations in sea ice related to varying influx of warm Atlantic waters into the Arctic basin (e.g., Werner et al., 2013).

A particularly high-resolution sea ice history has been established for the last 1,450 years using a network of terrestrial (tree ring and lake sediment) and ice-core records located around the margins of the Arctic (Kinnard et al., 2011). This network yields a history of summer sea ice minima during the pre- and post-industrial periods. Results indicate a pronounced decline in summer sea ice beginning in the 20th century with exceptionally low ice extent recorded since the mid-1990s (**Fig. 3**). While several episodes of reduced and expanded sea ice extent occur in association with climate anomalies such as the Medieval Climate Warm Period (AD 800-1300) and the Little Ice Age (AD 1450-1850), the extent and pace of the modern decline in sea ice is *outside of the range of natural variability and unprecedented in the 1450-year reconstruction* (Kinnard et al., 2011). The authors conclude that the pre-industrial sea ice climate signal (prior to anthropogenic forcing) was driven by a combination of changes in atmospheric temperature and circulation as well as variations in the inflow of warm saline Atlantic-sourced water masses through the Fram Strait. The significant post-industrial sea ice decline occurs in concert

with significant atmospheric and ocean warming driven by an exponential increase in atmospheric CO_2 (**Fig. 3**). High-resolution temperature proxy records from Arctic regions indicate that the modern rate of increasing surface air temperature has not been observed in at least the last 2000 years (McKay and Kaufman, 2014). Further, the Arctic Ocean has experienced intensified warming due to the increasing inflow of relatively warm Atlantic Waters from the Norwegian Sea into the Arctic basin (**Fig. 3**; Spielhagen et al., 2011). Using both ecology and geochemistry of foraminifera from a Fram Strait sediment core, scientists report a 2° C increase in inflowing water temperature since 1900.

The Arctic plays an important role in the Earth's climate; therefore, understanding and monitoring Arctic change is important to understanding and predicting global climate impacts. Over time scales of decades to tens of thousands of years, paleoclimate records indicate that sea ice extent over various time scales is forced by insolation, heat advection via ocean water inflows, atmospheric circulation and surface ocean temperatures. Some climate model projections suggest ice-free Arctic summers as early as 2030, and most scientists agree that such conditions are likely before the end of the 21st century. Rapid declines in sea ice extent and thickness reported over the last decades have been attributed to both anthropogenic climate change and natural climate variability. Over the past several decades, inflowing Atlantic waters have warmed and expanded in depth, and river discharge to the Arctic has increased, further driving sea ice melt and warming seas. While understanding the interplay of these factors is critical for future projections of Arctic sea ice and ecosystems, unfortunately most observational time-series records cover only a few decades. This highlights the need for additional paleoceanographic reconstructions of varying spatial and temporal coverage to better understand Arctic Ocean change.

Fig. 3. Paleoclimate reconstructions of approximately 5-year mean sea ice extent (Kinnard et al., 2011), atmospheric temperature (McKay and Kaufman, 2014) and sea surface temperature anomalies (Spielhagen et al., 2011) spanning the last 1,500 years. Atmospheric CO_2 concentrations from the Law Dome ice core record (Ethridge et al., 1996, 1998) and modern observations from the Mauna Loa observatory (Dr. Pieter Tans, NOAA/ESRL (www.esrl.noaa.gov/gmd/ccgg/trends/) and Dr. Ralph Keeling, Scripps Institution of Oceanography (scrippsco2.ucsd.edu/).Temperature anomalies are used to show the fluctuations in temperature around a long-term mean; positive anomalies indicate warmer than average temperatures within a time series. The vertical dashed black line marks the start of the Industrial Revolution and global impacts of anthropogenic carbon emissions.

References

Anagnostou, E., E. H. John, K. M. Edgar, et al., 2016: Changing atmospheric CO_2 concentration was the primary driver of early Cenozoic climate. *Nature*, 533, 380-384, doi: 10.1038/nature17423.

Beerling, D. J., and D. L Royer, 2011: Convergent Cenozoic CO_2 history. *Nature Geoscience*, 4, 418-420, doi: 10.1038/ngeo1186.

Cronin, T. M., L. Gemery, W. M. Briggs Jr., M. Jakobsson, L. Polyak, and E. M. Brouwers, 2010: Quaternary sea-ice history in the Arctic Ocean based on a new ostracode sea-ice proxy. *Quaternary Science Reviews*, 29, 3415-3429.

Cronin, T. M., L. Polyak, D. Reed, E. S. Kandiano, R. E. Marzen, and E. A. Council, 2013: A 600-kyr Arctic sea-ice record from Mendeleev Ridge based on ostracodes. *Quaternary Science Reviews*, 79, 157-167.

Darby, D. A., L. Polyak, and H.A. Bauch, 2006: Past glacial and interglacial conditions in the Arctic Ocean and marginal seas - a review. *Progress in Oceanography*, 71, 129-144.

Darby, D. A., 2008: The Arctic perennial ice cover over the last 14 million years. *Paleoceanography*, doi: 10.1029/2007PA001479.

Etheridge, D. M., L. P. Steele, R. L. Langenfelds, R. J Francey, J. -M. Barnola, and V. I. Morgan, 1996: Natural and anthropogenic changes in atmospheric CO_2 over the last 1000 years from air in Antarctic ice and firn. *Journal of Geophysical Research*, 101, 4115-4128.

Etheridge, D. M., L. P. Steele, R. J. Francey, and R. L. Langenfelds, 1998: Atmospheric methane between 1000 A.D. and present: Evidence of anthropogenic emissions and climatic variability. *Journal of Geophysical Research*, 103, 15,979-15,993.

Hörner, T., R. Stein, K. Fahl, and D. Birgel, 2016: Post-glacial variability of sea ice cover, river run-off and biological production in the western Laptev Sea (Arctic Ocean): A high-resolution biomarker study. *Quaternary Science Reviews*, 143, 133-149, doi: 10.1016/j.quascirev.2016.04.011.

Jakobsson, M., K. Andreassen, L. R. Bjarnadottir, et al., 2014: Arctic Ocean glacial history. *Quaternary Science Reviews*, 92, 40-67, doi: 10.1016/j.quascirev.2013.07.033.

Jakobsson, M., J. Nilsson, L. Anderson, et al., 2016: Evidence for an ice shelf covering the central Arctic Ocean during the penultimate glaciation. *Nature Communications*, 7, 10365, doi: 10.1038/ncomms10365.

Kinnard, C., C. M. Zdanowicz, D. A. Fisher, E. Isaksson, A. de Vernal, and L. G. Thompson, 2011: Reconstructed change in Arctic sea ice over the last 1,450 years. *Nature*, 479, 509-512, doi: 10.1038/nature10581.

McKay, N. P., and D. S. Kaufman, 2014: An extended Arctic proxy temperature database for the past 2,000 years. *Scientific Data*, 1, 140026, doi: 10.1038/sdata.2014.26.

Marzen, R. E., L. H. DeNinno, and T. M. Cronin, 2016: Calcareaous microfossil-based orbital cyclostratigraphy in the Arctic. *Quaternary Science Reviews*, 149, 109-121.

Müller, J., K. Werner, R. Stein, K. Fahl, M. Moros, and E. Jansen, 2012: Holocene cooling culminates in sea ice oscillations in Fram Strait. *Quaternary Science Reviews*, 47, 1-14, doi: 10.1016/j.quascirev.2012.04.024.

O'Regan, M., K. St. John, K. Moran, et al., 2010: Plio-Pleistocene trends in ice rafted debris on the Lomonosov Ridge. *Quaternary International*, 219, 169-176, doi: 10.1016/j.quaint.2009.08.010.

Polyak, L., R. B. Alley, J. T. Andrews, et al., 2010: History of sea ice in the Arctic. *Quaternary Science Reviews*, 29, 1757-1778.

Polyak, L., K. Best, K. Crawford, E. Council, and G. St-Onge, 2013: Quaternary history of sea ice in the western Arctic Ocean based on foraminifera. *Quaternary Science Reviews*, 79, 145-156.

Polyak, L., S. T. Belt, P. Cabedo-Sanz, M. Yamamoto, and Y. -H. Park, 2016: Holocene sea-ice conditions and circulation at the Chukchi-Alaskan margin, Arctic Ocean, inferred from biomarker proxies. *The Holocene*, 26, 1810-1821, doi: 10.1177/0959683616645939.

St. John, K., 2008: Cenozoic ice-rafting history of the central Arctic Ocean: Terrigenous sands on the Lomonosov Ridge. *Paleoceanography*, 23, PA1S05.

Spielhagen, R. F., K. Werner, S. A. Sorensen, et al., 2011: Enhanced modern heat transfer to the Arctic by warm Atlantic water. *Science*, 311, 450-453.

Stein, R., K. Fahl, and J. Muller, 2012: Proxy reconstruction of Arctic Ocean sea ice history: 'From IRD to IP_{25}'. *Polarforschung*, 82, 37-71.

Stein, R., K. Fahl, I. Schade, A. Manerung, S. Wassmuth, F. Niessen, S. -I. Nam, 2017: Holocene variability in sea ice cover, primary production, and Pacific-Water inflow and climate change in the Chukchi and East Siberian Seas (Arctic Ocean). *Journal of Quaternary Science*, 32, 362-379.

Stickley, C. E., K. St. John, N. Koç, R. W. Jordan, S. Passchier, R. B. Pearce, and L. E. Kearns, 2009: Evidence for middle Eocene Arctic sea ice from diatoms and ice-rafted debris. *Nature*, 460, 376-379.

Vare, L. L., G. Masse, T. R. Gregory, C. W. Smart, and S. T. Belt, 2009: Sea ice variations in the central Canadian Arctic Archipelago during the Holocene. *Quaternary Science Reviews*, 28, 1354-1366, doi: 10.1016/j.quascirev.2009.01.013.

Werner, K., R. F. Spielhagen, D. Bauch, H. C. Hass, and E. Kandiano, 2013: Atlantic Water advection versus sea-ice advances in the eastern Fram Strait during the last 9 ka: Multiproxy evidence for a two-phase Holocene. *Paleoceanography*, 28, 283-295, doi: 10.1002/palo.20028.

Woodgate, R. A., T. J. Weingartner, and R. Lindsay, 2010: The 2007 Bering Strait oceanic heat flux and anomalous Arctic sea-ice retreat. *Geophysical Research Letters*, 37, L01602.

Zhang, Y. G., M. Pagani, Z. Liu, S. M. Bohaty, and R. DeCanto, 2013: A 40-million-year history of atmospheric CO_2. *Philosophical Transactions of the Royal Society A*, 371, 20130096, doi: 10.1098/rsta.2013.0096.

December 4, 2017

Collecting Environmental Intelligence in the New Arctic

J. T. Mathis[1], E. Osborne[1], S. Starkweather[2]

[1]NOAA Arctic Research Program, Office of Oceanic and Atmospheric Research, 1315 East West Highway, Silver Spring, MD 20910, USA

[2]Cooperative Institute for Research in Environmental Sciences, 216 UCB, University of Colorado Boulder, Boulder, CO 8030, USA

Highlights

- Rapid environmental transitions in the Arctic highlight the need for a swift and responsive approach to scientific observing and interpretation.
- Addressing the need to produce timely and relevant scientific results, Environmental Intelligence (EI) is the production of integrated environmental knowledge from observations, modeling, and data integrations that links researchers, stakeholder and decision-makers in an iterative process.
- Application of the EI framework to an ocean acidification and Alaskan fisheries case study provides a proof of concept of the EI cycle.

Shortly after the beginning of the 21st Century, the Arctic began an environmental transition so extensive that it caught scientists, policymakers, and residents by surprise. The extent and duration of these transitions define the New Arctic, characterized by the lowest winter maximum in sea ice cover on record for 2017, the persistent and record warming of sea surface temperatures across the Arctic, and the downward trend in total ice mass of the Greenland ice sheet, just to name a few. The unprecedented rate and global reach of these changes highlight the pressing need to prepare for and adapt to the New Arctic. Historically, Arctic data have been collected through regional process studies, due to the prohibitive costs and logistical challenges of measuring at a system-wide scale. Given the urgent need for environmental information in the Arctic, scientists must now take a different approach to Arctic observing. By developing and using the Environmental Intelligence (EI) framework we aim to achieve the end-to-end integration of research across linked and iterative steps of scientific research and decision support. By integrating across Arctic system observing, data integration and modeling efforts, scientific results can be more responsive to stakeholder needs and policy-relevant. The EI approach aims to produce environmental knowledge that is timely, reliable, and suitable for decision support at the local, state, and national levels.

Environmental Intelligence Cycle

The sparseness of observations and limited seasonal coverage of in situ EI gathering has limited our ability to fully understand the dynamics of the New Arctic. Emerging challenges regarding Arctic change are globally important and include changes in Northern Hemisphere weather patterns, ecosystem and fisheries stability, sea level rise, economic development, maritime safety, and national security. To effectively study these issues,

the EI framework can be applied to specific environmental issues or focused on the development of actionable environmental knowledge.

The EI Cycle (**Fig. 1**) starts with the identification of relevant stakeholders and decision support objectives, culminating in the determination of an environmental focus area. The next step in the cycle aims to harness existing data archives that can be leveraged to increase the spatial and temporal understanding of the environmental focus area. Identified datasets are translated into functional evidence that can then be used to identify observing gaps and to strategically enhance observing efforts. Integration of the data and observing efforts provide the best system-wide dataset available that can then be used to validate systems-level models. The modeling component of the EI cycle is critical as modeling is a vital tool to advancing system integration, capturing feedbacks within the system and projecting current trends into the future. Therefore, data integration and observing systems should focus on collecting suitable data that can enhance model outputs. The final steps of the EI cycle assess the effectiveness of new environmental knowledge for stakeholder needs and provide options for action to decision-makers.

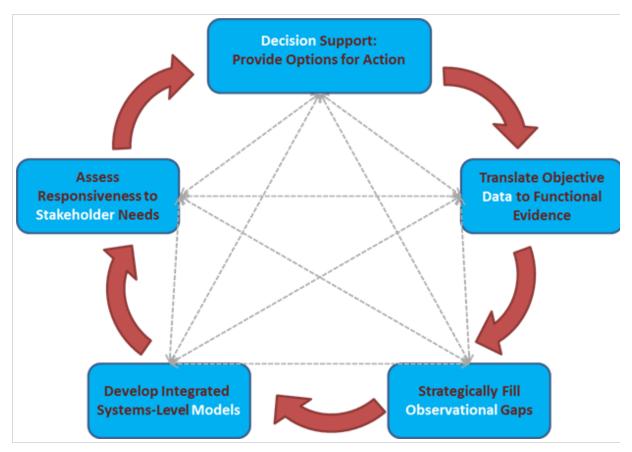**Fig. 1.** Environmental Intelligence Cycle showing the iterative steps of intelligence gathering.

An important characteristic of the EI framework is that it is iterative, meaning the process can move quickly through its steps while still revisiting previous steps later that allow the process to be responsive to the immediate needs at hand. Specifically, the final steps of assessment and decision support often lead to new

issues that need to be investigated by the research components of the EI framework. One of the most critical components of the EI construct is the seamless and continuous integration of data, observations and modeling. Disconnects between these steps can lead to inefficiencies and breakdown of the cycle as resources and outcomes become compartmentalized and not well integrated.

When possible, EI should be gathered at as many temporal and spatial scales as possible by using a nested observing framework (**Fig. 2**). By integrating data collection across a number of platforms—from satellites that can cover large swaths of the Arctic to community-based observers on the ground—actionable information can be gathered more efficiently. The EI Cycle prioritizes the exchange of knowledge between researchers and stakeholders, as this is critical to assessing the responsiveness of investments in data management, observing and modeling. Improvements within and across each of these areas will improve the ability to understand, communicate about, and support decisions in response to the impacts of Arctic change. These efforts, across the scales from community to global, are now of the utmost importance.

Fig. 2. A nested observing framework (adapted from Alessa et al., 2015, **Fig. 1**) can be applied for the observational steps of the Environmental Intelligence cycle. The base of the pyramid is made up of observing platforms that have the highest spatial coverage (e.g., satellites), but oftentimes the lowest resolution. In stepping up through the pyramid through platforms such as aircraft, land-based observatories, ocean drones and finally community-based observers, the data coverage becomes constrained, but the resolution is greater.

Societal Benefit Areas

The science of what is driving the changes in the Arctic is becoming clearer. However, we need to expand and improve sustained information gathering to provide actionable intelligence and forecasting needed by people of the Arctic and other stakeholders. The issues at stake include food security, cultural survival, environmental and community health as well as emerging opportunities in commerce, trade and issues of national security.

One highly effective way of doing this is to develop EI gathering around societal benefit areas (**Table 1**), Societal benefit areas can help frame knowledge development that is multi-disciplinary, highly relevant to stakeholder needs, and perhaps most importantly, actionable (IDA Science and Technology Policy Institute and Sustaining Arctic Observing Networks, 2017). The societal benefit areas reveal how values to society accrue the observations and value-added research efforts, like modeling and product development. As such, they can transcend national efforts, making it easier to develop functional evidence that is internationally relevant.

Table 1. Societal Benefit Areas for the Arctic, as identified in 2016 through collaborations between the U.S. Science and Technology Policy Institute (STPI) and the international Sustaining Arctic Observing Networks (SAON).

- Disaster Preparedness
- Environmental Quality
- Food Security
- Fundamental Understanding of Arctic Systems
- Human Health
- Infrastructure and Operations
- Marine and Coastal Ecosystems and Processes
- Natural Resources
- Resilient Communities
- Sociocultural Services
- Terrestrial and Freshwater Ecosystems and Processes
- Weather and Climate

A Case Study

To assess the effectiveness of utilizing the EI framework, it was applied to a 2014 study evaluating the effects of ocean acidification on Alaskan fisheries and economies. Ocean acidification (OA) is defined as the progressive decline in ocean pH that is caused by the accumulation of anthropogenic carbon dioxide (CO_2) in seawater. The Arctic and subarctic seas are especially vulnerable to OA because a number of natural and human process act in concert to drive down pH and dissolved carbonate mineral concentrations (Mathis et al., 2015b). Alaskan Arctic organisms that strongly depend on dissolved carbonate include crabs, mussels and the low trophic-level organisms like pteropods that are an important food source for finfish such as salmon (Bednaršek et al., 2014). The vastness of areas potentially impacted by OA in the Alaskan Arctic and the associated disruptions to commercial and subsistence fisheries required a unique approach to collect environmental intelligence on this issue.

Following the EI framework, relevant stakeholders and decision support objectives were identified. In this case, a commercial shellfish hatchery in Southern Alaska needed to know if conditions were and would remain conducive for successful operation. This aligned with several key societal benefit areas (**Table 1**) including environmental quality, food security, marine and coastal ecosystem processes and resilient communities. This issue was also important to regional management and state and Federal policymakers due to the emergent aquaculture industry in Alaska.

The project then moved into translating objective, available data into functional evidence. In this case, there was little environmental knowledge about OA in Alaska, but there were socio-economic data that showed that Alaska seafood is a primary source of protein for 30-46% of residents of the state (Frisch et al., 2014).

With an understanding of the functional evidence, the project moved on to strategically fill observational gaps, with specific consideration as to how those observations could be used in the future step of developing systems-level models. Given the lack of actionable intelligence about OA in Alaska, an extensive observational campaign was put into place that collected millions of ocean observations at varying temporal and spatial scales. Some of these observing systems were deployed at a high intensity for a few days over a wide area (i.e., a ship-based survey), while others were deployed for several months at shore-based facilities. Observations were focused in the region adjacent to the shellfish hatchery as well as across the entire Gulf of Alaska for model development and validation activities. The data collected as a part of this observational campaign showed that OA was a chronic environmental stressor (Evans et al., 2014).

Using the new observational results, a systems-level model was developed for the region to assess the impacts of natural and anthropogenic drivers of OA that affect the Alaskan hatchery. The model outputs indicated that currently there is a 5-month window of optimal growing conditions for many juvenile shellfish species. However, model projections indicate that window is expected to close entirely by 2040 (Evans et al., 2015). The model was scaled up to a regional level for other shellfish hatcheries within the Gulf of Alaska that also needed environmental intelligence for their operations. This regional model showed similar outcomes for OA, with conditions becoming challenging for shellfish growth in hatcheries without mitigation efforts by the year 2100 (Siedlecki et al., 2017).

Completing the EI Cycle, we returned to the initial step of our EI case study to determine responsiveness to stakeholder needs. A fully developed risk assessment was established for Alaskan fisheries using the environmental knowledge gathered as a part of this study. These new insights showed that Alaskan commercial and subsistence fisheries are located in seas projected to experience rapid transitions in temperature, pH, and other chemical parameters caused by global change, especially OA. Many of the marine organisms that are most intensely affected by OA, such as mollusks, contribute substantially to the state's highly productive commercial fisheries and traditional subsistence way of life (Mathis et al., 2015a).

The outcome of this first trip through the EI cycle did address the needs identified at the outset of the EI Cycle and supported a number of societal benefit areas. However, the results also identified more decision support areas, which is exactly how the EI Cycle is supposed to work. In this case, from start to finish, the first iteration of the EI Cycle took approximately 18 months, but the project continues today as more environmental knowledge

is generated. The faster a project can move through each round of the EI Cycle, the more responsive it can be to both identifying and addressing stakeholder needs and societal benefits.

Final Thoughts

Global connections to Arctic change are becoming more pronounced, including sea level rise and the propagation of extreme weather events into lower latitudes. It is clear that the New Arctic brings challenges as well as opportunities. In recent years, the Arctic has undergone unprecedented transitions and trends show a clear, stronger and more pronounced signal of persistent warming than at any point in our observational record to at least the late 1800s. The rate and magnitude of these changes challenge the Arctic community to expand and improve sustained information gathering to more effectively provide actionable intelligence and forecasting needed by residents and stakeholders. As shown in the OA case study, the use of the EI Cycle is a highly effective way to respond to the rapid transitions that are underway. Other issues at stake that could benefit from the EI framework include food security, cultural survival, and community health, along with emerging opportunities in commerce and trade.

References

Alessa, L., A. Kliskey, J. Gamble, M. Fidel, G. Beaujean, and J. Gosz, 2015: The role of Indigenous science and local knowledge in integrated observing systems: moving toward adaptive capacity indices and early warning systems. *Sustain Sci.*, 11, 91-102, doi: 10.1007/s11625-015-0295-7.

Bednaršek, N., G. A. Tarling, D. C. E. Bakker, S. Fielding, and R. A Feely, 2014: Dissolution dominating calcification process in polar pteropods close to the point of aragonite undersaturation. *PLoS One*, Vol. 9, Issue 10.

Evans, W., J. T. Mathis, and J. N. Cross, 2014: Calcium carbonate corrosivity in an Alaskan Inland Sea. *Biogeosciences*, 11, 365–379, doi: 10.5194/bg-11-365-2014.

Evans, W., J. T. Mathis, J. Ramsey, and J. Hetrick, 2015: On the frontline: Tracking $CaCO_3$ corrosivity in an Alaskan shellfish hatchery. *PLoS One*, 10(7), e0130384, doi: 10.1371/journal.pone.0130384.

Frisch, L. C., J. T. Mathis, N. P. Kettle, and S. Trainor, 2014: Gauging perceptions of ocean acidification in Alaska. *Marine Policy*, 53, 101-110, doi: 10.1016/j.marpol.2014.11.022.

IDA Science and Technology Policy Institute and Sustaining Arctic Observing Networks. 2017: International Arctic Observations Assessment Framework. IDA Science and Technology Policy Institute, Washington, DC, U.S.A., and Sustaining Arctic Observing Networks, Oslo, Norway, 73 pp.

Mathis, J. T., S. R. Cooley, N. Lucey, S. Colt, J. Ekstrom, T. Hurst, C. Hauri, W. Evans, J. N. Cross, and R. A. Feely, 2015a: Ocean acidification risk assessment for Alaska's fishery sector. *Progress in Oceanography*, 136, 71-91, doi: 10.1016/j.pocean.2014.07.001.

Mathis, J. T., J. N. Cross, W. Evans, and S. Doney, 2015b: Ocean acidification in the surface waters of the Pacific-Arctic boundary regions. *Oceanography*, 28(2), 122-135, doi: 10.5670/oceanog.2015.36.

Siedlecki, S. A., D. J. Pilcher, A. J. Hermann, K. Coyle, and J. Mathis, 2017: The importance of freshwater to spatial variability of aragonite saturation state in the Gulf of Alaska. *Journal of Geophysical Research: Oceans*, 122, https://doi.org/10.1002/2017JC012791.

January 5, 2018

Authors and Affiliations

U. S. Bhatt, Geophysical Institute, University of Alaska Fairbanks, Fairbanks, AK, USA

J. Bjerke, Norwegian Institute for Nature Research, Tromsø, Norway

J. E. Box, Geological Survey of Denmark and Greenland, Copenhagen, Denmark

R. Brown, Climate Research Division, Environment and Climate Change Canada, Canada

J. Cappelen, Danish Meteorological Institute, Copenhagen, Denmark

H. H. Christiansen, Geology Department, University Centre in Svalbard, UNIS, Norway

J. C. Comiso, Cryospheric Sciences Laboratory, NASA Goddard Space Flight Center, Greenbelt, MD, USA

L. W. Cooper, Chesapeake Biological Laboratory, University of Maryland Center for Environmental Science, Solomons, MD, USA

T. Cronin, U.S. Geological Survey, Reston, VA, USA

C. Derksen, Climate Research Division, Environment and Climate Change Canada, Canada

C. Dickerson, Department of Environmental Sciences, University of Virginia, Charlottesville, VA, USA

D. S. Drozdov, Earth Cryosphere Institute, Tyumen Science Center, Tyumen, Russia; Tyumen State University, Tyumen, Russia

L. B. Eisner, Alaska Fisheries Science Center, NOAA, Seattle, WA, USA

H. Epstein, Department of Environmental Sciences, University of Virginia, Charlottesville, VA, USA

J. Farmer, Princeton University - Department of Geosciences, Princeton, NJ, USA

S. Farrell, NOAA Earth System Science Interdisciplinary Center, University of Maryland, College Park, MD, USA

P. Fauchald, Norwegian Institute for Nature Research, Tromsø, Norway

R. S. Fausto, Geological Survey of Denmark and Greenland, Copenhagen, Denmark

X. Fettweis, University of Liege, Liege, Belgium

B. C. Forbes, Arctic Centre, University of Lapland, Rovaniemi, Finland

K. E. Frey, Graduate School of Geography, Clark University, Worcester, MA, USA

S. Gerland, Norwegian Polar Institute, Fram Centre, Tromsø, Norway

R. R. Gradinger, UiT, The Arctic University of Norway, Tromsø, Norway

J. M. Grebmeier, Chesapeake Biological Laboratory, University of Maryland Center for Environmental Science, Solomons, MD, USA

C. Haas, Alfred Wegener Institute, Helmholtz Centre for Polar and Marine Research, Bremerhaven, Germany

E. Hanna, Department of Geography, University of Lincoln, Lincoln, UK

K. Hansen, Geological Survey of Denmark and Greenland, Copenhagen, Denmark

I. Hanssen-Bauer, Norwegian Meteorological Institute, Blindern, 0313 Oslo, Norway

S. Helfrich, NOAA/NESDIS Center for Satellite Applications and Research, USA

S. Hendricks, Alfred Wegener Institute, Helmholtz Centre for Polar and Marine Research, Bremerhaven, Germany

K. Holsman, Resource Ecology and Fisheries Management Division, Alaska Fisheries Science Center, National Marine Fisheries Service, National Oceanic and Atmospheric Administration, 7600 Sand Point Way NE, Seattle, WA 98115, USA

T. Horstkotte, Department of Ecology and Environmental Sciences, Umeå University, Umeå, Sweden

J. Ianelli, Resource Ecology and Fisheries Management Division, Alaska Fisheries Science Center, National Marine Fisheries Service, National Oceanic and Atmospheric Administration, 7600 Sand Point Way NE, Seattle, WA 98115, USA

K. Isaksen, Norwegian Meteorological Institute, Oslo, Norway

A. L. Kholodov, Geophysical Institute, University of Alaska Fairbanks, Fairbanks, AK, USA

S. -J. Kim, Korea Polar Research Institute, Incheon, Republic of Korea

T. Krumpen, Alfred Wegener Institute, Helmholtz Centre for Polar and Marine Research, Bremerhaven, Germany

C. Ladd, Pacific Marine Environmental Laboratory, NOAA, Seattle, WA, USA

K. Luojus, Arctic Research Centre, Finnish Meteorological Institute, Finland

M. Macias-Fauria, School of Geography and the Environment, Oxford University, Oxford, UK

G. V. Malkova, Earth Cryosphere Institute, Tyumen Science Center, Tyumen, Russia

S. S. Marchenko, Geophysical Institute, University of Alaska Fairbanks, Fairbanks, AK, USA

A. Martin, Department of Zoology, Oxford University, Oxford, UK

J. T. Mathis, NOAA Arctic Research Program, Office of Oceanic and Atmospheric Research, 1315 East West Highway, Silver Spring, MD 20910, USA

W. Meier, National Snow and Ice Data Center, Boulder, CO, USA

T. Mote, Department of Geography, University of Georgia, Athens, Georgia, USA

L. Mudryk, Climate Research Division, Environment and Climate Change Canada, Canada

R. Myneni, Department of Earth and Environment, Boston University, Boston, MA, USA

E. Osborne, NOAA Arctic Research Program, Office of Oceanic and Atmospheric Research, 1315 East West Highway, Silver Spring, MD 20910, USA

J. E. Overland, National Oceanic and Atmospheric Administration, Pacific Marine Environmental Laboratory, Seattle, WA, USA

D. Perovich, Thayer School of Engineering, Dartmouth College, Hanover, NH, USA

G. Phoenix, Department of Animal and Plant Sciences, University of Sheffield, Sheffield, UK

C. Polashenski, Thayer School of Engineering, Dartmouth College, Hanover, NH, USA; ERDC - CRREL, 72 Lyme Road, Hanover, NH, USA

M. Raynolds, Institute of Arctic Biology, University of Alaska Fairbanks, Fairbanks, AK, USA

J. Richter-Menge, University of Alaska Fairbanks, Institute of Northern Engineering, Fairbanks, AK, USA

R. Ricker, Alfred Wegener Institute, Helmholtz Centre for Polar and Marine Research, Bremerhaven, Germany

V. E. Romanovsky, Geophysical Institute, University of Alaska Fairbanks, Fairbanks, AK, USA

I. Sasgen, Climate Sciences Department, Alfred Wegener Institute, Bremerhaven, Germany

N. I. Shiklomanov, Department of Geography, George Washington University, Washington, DC, USA

E. Siddon, Auke Bay Laboratories, Alaska Fisheries Science Center, National Marine Fisheries Service, National Oceanic and Atmospheric Administration, 17109 Point Lena Loop Rd, Juneau, AK 99801, USA

C. J. P. P. Smeets, Institute for Marine and Atmospheric Research Utrecht, Utrecht University, Utrecht, The Netherlands

S. L. Smith, Geological Survey of Canada, Natural Resources Canada, Ottawa, ON, Canada

S. Starkweather, Cooperative Institute for Research in Environmental Sciences, 216 UCB, University of Colorado Boulder campus, Boulder, CO 80309, USA

D. A. Streletskiy, Department of Geography, George Washington University, Washington, DC, USA

M. Tedesco, Lamont Doherty Earth Observatory of Columbia University, Palisades, NY, USA; NASA Goddard Institute of Space Studies, New York, NY, USA

R. L. Thoman, NOAA, National Weather Service, Alaska Region, Anchorage, AK, USA

M. -L. Timmermans, Yale University, New Haven, CT, USA

H. Tømmervik, Norwegian Institute for Nature Research, Tromsø, Norway

J. -É. Tremblay, Québec-Océan and Takuvik, Biology Department, Université Laval, Québec City, QC, Canada

M. Tschudi, Aerospace Engineering Sciences, University of Colorado, Boulder, CO, USA

D. van As, Geological Survey of Denmark and Greenland, Copenhagen, Denmark

R. S. W. van de Wal, Institute for Marine and Atmospheric Research Utrecht, Utrecht University, Utrecht, The Netherlands

I. Velicogna, Department of Earth System Science, University of California, Irvine, California, USA

H. Vickers, Norut Northern Research Institute, Tromsø, Norway

D. Walker, Institute of Arctic Biology, University of Alaska Fairbanks, Fairbanks, AK, USA

J. E. Walsh, International Arctic Research Center, University of Alaska Fairbanks, Fairbanks, AK, USA

M. Wang, Joint Institute for the Study of the Atmosphere and Ocean, University of Washington, Seattle, WA, USA

M. Webster, NASA Goddard Space Flight Center, Greenbelt, MD, USA

A. Whitehouse, Resource Ecology and Fisheries Management Division, Alaska Fisheries Science Center, National Marine Fisheries Service, National Oceanic and Atmospheric Administration, 7600 Sand Point Way NE, Seattle, WA 98115, USA

K. Wood, Pacific Marine Environmental Laboratory, NOAA, Seattle, WA, USA

A. York, Alaska Fire Science Consortium, International Arctic Research Center, University of Alaska, Fairbanks, AK, USA

S. Zador, Resource Ecology and Fisheries Management Division, Alaska Fisheries Science Center, National Marine Fisheries Service, National Oceanic and Atmospheric Administration, 7600 Sand Point Way NE, Seattle, WA 98115, USA

R. Ziel, Alaska Fire Science Consortium, International Arctic Research Center, University of Alaska, Fairbanks, AK, USA